AD-A157 456 SIMPLODE: AN IMPLODING GAS PUFF PLASMA MODEL I NEON(U) 1/1
NAVAL RESEARCH LAB WASHINGTON DC J DAVIS ET AL.
26 JUL 85 NRL-MR-5615

UNCLASSIFIED F/G 20/9 NL

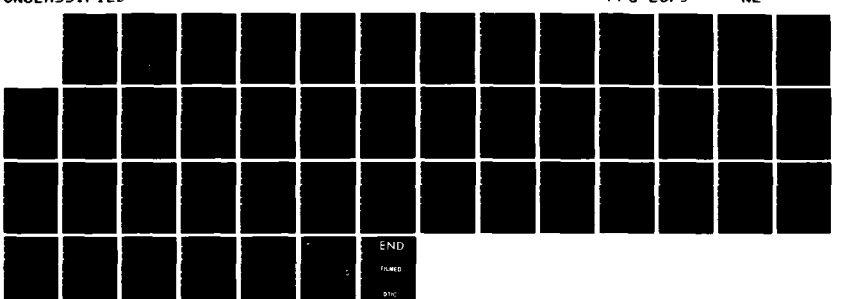

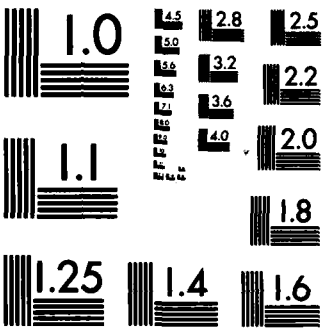

MICROCOPY RESOLUTION TEST CHART

NRL Memorandum Report 5615

SIMPLODE:
An Imploding Gas Puff Plasma Model
I. Neon

J. DAVIS, C. AGRITELLIS AND D. DUSTON

Plasma Radiation Branch
Plasma Physics Division

July 26, 1985

This research was sponsored by the Defense Nuclear Agency under Subtask T99QAXLA, work unit 00004 and work unit title "Advanced Simulation Concepts."

NAVAL RESEARCH LABORATORY
Washington, D.C.

SECURITY CLASSIFICATION OF THIS PAGE

REPORT DOCUMENTATION PAGE

1a REPORT SECURITY CLASSIFICATION UNCLASSIFIED	1b RESTRICTIVE MARKINGS
2a SECURITY CLASSIFICATION AUTHORITY	3 DISTRIBUTION / AVAILABILITY OF REPORT
2b DECLASSIFICATION / DOWNGRADING SCHEDULE	Approved for public release; distribution unlimited.
4 PERFORMING ORGANIZATION REPORT NUMBER(S) NRL Memorandum Report 5615	5 MONITORING ORGANIZATION REPORT NUMBER(S)
6a NAME OF PERFORMING ORGANIZATION Naval Research Laboratory 6b OFFICE SYMBOL (If applicable) Code 4720	7a NAME OF MONITORING ORGANIZATION Defense Nuclear Agency
6c ADDRESS (City, State, and ZIP Code) Washington, DC 20375-5000	7b ADDRESS (City, State, and ZIP Code) Washington, DC 20305
8a NAME OF FUNDING / SPONSORING ORGANIZATION Defense Nuclear Agency 8b OFFICE SYMBOL (If applicable) RAEV	9 PROCUREMENT INSTRUMENT IDENTIFICATION NUMBER
8c ADDRESS (City, State, and ZIP Code) Washington, DC 20305	10 SOURCE OF FUNDING NUMBERS PROGRAM ELEMENT NO. 62715H; PROJECT NO.; TASK NO.; WORK UNIT ACCESSION NO. DN880-191

11 TITLE (Include Security Classification)
SIMPLODE: An Imploding Gas Puff Plasma Model — I. Neon

12 PERSONAL AUTHOR(S)
Davis, J., Agritellis, C. and Duston, D.

13a TYPE OF REPORT	13b TIME COVERED	14 DATE OF REPORT (Year, Month, Day)	15 PAGE COUNT
Interim	FROM 10/84 TO 10/85	1985 July 26	46

16 SUPPLEMENTARY NOTATION
This research was sponsored by the Defense Nuclear Agency under Subtask T99QAXLA, work unit 00004 and work unit title "Advanced Simulation Concepts."

17 COSATI CODES			18 SUBJECT TERMS (Continue on reverse if necessary and identify by block number)
FIELD	GROUP	SUB-GROUP	SIMPLODE, Neon, Implosion, Gas Puff

19 ABSTRACT (Continue on reverse if necessary and identify by block number)

A non-LTE dynamic pinch model - SIMPLODE - has been developed and applied to describing the implosion dynamics of a K-shell radiating gas puff. Numerical simulations have been carried out with neon gas puffs and compared with recent experimental results obtained on GAMBLE II. In addition, the influence of the Plasma Erosion Opening Switch on the K-shell yield is investigated. Keywords:

20 DISTRIBUTION / AVAILABILITY OF ABSTRACT	21 ABSTRACT SECURITY CLASSIFICATION
☒ UNCLASSIFIED/UNLIMITED ☐ SAME AS RPT ☐ DTIC USERS	UNCLASSIFIED
22a NAME OF RESPONSIBLE INDIVIDUAL J. Davis	22b TELEPHONE (Include Area Code) (202) 767-3278 22c OFFICE SYMBOL Code 4720

DD FORM 1473, 84 MAR 83 APR edition may be used until exhausted
All other editions are obsolete

SECURITY CLASSIFICATION OF THIS PAGE

CONTENTS

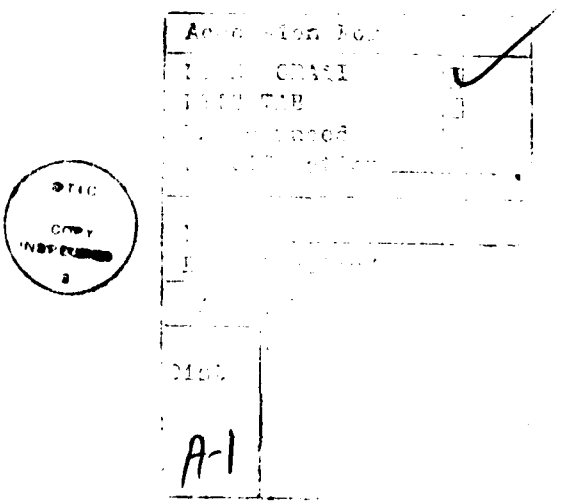

SIMPLODE:
AN IMPLODING GAS PUFF PLASMA MODEL
I. NEON

I. INTRODUCTION

The use of a gas puff plasma as a transducer for the conversion of electrical to radiative energy has been the focus of an intense experimental and theoretical program for the past several years. Although a considerable amount of electrical and spectral data has been generated the bulk of it remains uncorrelated and unanalyzed. Only for those shots where the radiative yield was considered impressive has there been any analysis. Generally, the "analysis" provided information on the average plasma temperature and density from emission spectra, plasma size from x-ray pinhole photos and total radiative yield from calorimetry. Based on this "analysis" it would be difficult to obtain anything but the most rudimentary understanding of the plasma dynamics, certainly not enough to allow the systematic selection of both the machine parameters and load characteristics that would predict an optimum radiative yield shot.

The theory effort is chartered to develop a variety of theoretical models, tools, and numerical simulations to understand, guide, and predict the behavior of these high brightness laboratory x-ray sources. The models vary from the simple 0-D hydrodynamic implosion schemes to the complex and sophisticated 2-D Non-LTE radiation magnetohydrodynamic numerical simulations. These models have recently been used successfully for analysis and interpretation of several past and present experiments as well as for scaling to higher energy systems.[1-3] For this investigation it was essential to have a theoretical capability that would provide, in real time, an interactive link between theory and experiment. This requirement precluded the use of the more sophisticated numerical models which required large continuous intervals of computer time, which was unavailable, and therefore dictated the application of a less

Manuscript approved May 1, 1985.

sophisticated model but one that included some of the relevant physics. The SIMPLODE model satisfies these requirements. Briefly, the SIMPLODE model describes the O-D implosion dynamics of a current driven plasma slug self-consistently coupled to a Non-LTE radiation physics model and is ideal for use with the gas puff experiments at NRL on the GAMBLE II facility.

Recently the GAMBLE II pulse power facility has been upgraded to accomodate gas puff loads. This modification enhances GAMBLE II's versatility by expanding the types of material loads that can be investigated on it making the facility very attractive for examining Plasma Radiation Source (PRS) Loads. The inaugural series of experiments involved krypton, argon, and neon with most of the work being devoted to neon. These experiments were designed to calibrate the facility and determine its performance level in dealing with gas puff loads and nozzle technology. Also, neon was a better matched load for GAMBLE II in terms of the efficient conversion of electrical energy to K-shell radiation. Another aspect of the GAMBLE II experiments was to examine the impact of sharper current risetime on the implosion dynamics and radiative yields.

The work presented here will be concerned primarily with some of the theoretical aspects of the neon gas puff plasmas. In particular, the dynamic and radiative characteristics of the implosion as a function of input parameters. A comparison with some of the experimental results will be made. A report describing the majority of the experiments is currently in preparation in conjunction with the Plasma Technology Branch and is forthcoming.

II. Model

The simplest description of an imploding Z-pinch plasma is probably the Bennet pinch equilibrium model.[4] It represents an equilibrium balance between the fluid and the magnetic pressures in combination with an equilibrium balance between the energy in and the energy out. The obvious extension to the Bennet

equilibrium pinch model is the inclusion of flow parameters following the temporal evolution of the plasma, i.e., maintain the simple philosophy of the Bennet pinch but allow the plasma to evolve in time. In essence, this is our philosophy - a dynamic Bennet pinch. Also, like Shearer,[5] who included a radiation cooling term in the form of bremsstrahlung losses, we also include radiation cooling but in a more extensive fashion. The radiation cooling term in our model includes contributions from free-free, free-bound, and bound-bound transitions and are determined from a Non-LTE collisional-radiative model of the ionization dynamics.[3]

The model - SIMPLODE - treats a cylindrical annular gas puff plasma of uniform density carrying a uniform current in the Z-direction. Only the radial motion is considered - hence, the plasma is always uniform in the Z-direction, i.e., no axial structure. The radial acceleration is determined from the force equation, vig.

$$m\dot{u} = \left(P - \frac{I^2}{2\pi r^2 c^2}\right) A \qquad (1)$$

where $\dot{r} = \frac{dr}{dt} = u$ and $\ddot{r} = \dot{u}$, P is the fluid pressure, A is the area over which the force is exerted, i.e., $2\pi r\ell$, and $I^2/2\pi r^2c^2$ is the magnetic pressure, i.e., $B^2/8\pi$. The thermal energy, $E_{th} = \frac{3}{2}(1+z)NkT + \Sigma\mu_p$, varies in time as

$$\dot{E}_{th} = -\frac{P}{N}\left(\frac{\dot{V}}{V}\right) + \frac{\eta I^2}{A_{curr}}\ell - P_{rad}V \qquad (2)$$

where $\Sigma\mu_p$ is essentially the sum of ionization energies and is sometimes loosely referred to as chemical potential. $A_{curr} = \pi(R_o^2 - R_i^2)$ where $R_o(R_i)$ represent the outer (inner) radius of the plasma, $\dot{V} = 2\pi\ell r\dot{r}$, $N = \frac{m/m_i}{\pi r^2 \ell}$ where m is the mass, m_i the atomic mass and the thermal pressure is N(1+z)kT. The first term on the RHS of Eq. (2) represents the work done in compressing the plasma, the second term is the joule heating source, and the third term is the power radiated per unit volume from the

volume V. n represents classical resistivity, and ℓ the plasma length. The self-consistent solution to these equations is what we refer to as SIMPLODE. In the absence of a circuit model, $\dot{I}$ (= current waveform) is determined experimentally and used as an input parameter. [The model is presently being extended to evaluate self-consistently the current from a circuit model based on the open circuit voltage.] It is not yet clear that there are any significant differences between the current waveform as recorded from the current monitors and the theoretically calculated current waveform, except at late time, i.e., well after peak current, where the current crowbars and does not vanish on the experimental waveform. If taken seriously, it can maintain the plasma in a heated compressed state and overestimate the radiative losses, i.e., predict a higher yield. Hence, the input current waveforms have been reduced to zero at late time to avoid overestimating the yield.

III. Results and Discussion

Since most of the experiments were done with neon gas puffs, the numerical simulations will also focus on neon. In addition, the experiments were divided into two categories: with and without the Plasma Erosion Opening Switch (PEOS). To differentiate between the categories we will generally refer to them as the switch and no-switch cases, respectively. However, when the PEOS was included both the peak current and current waveform were substantially different from the no-switch case. In fact, the peak current only achieved 70% of the no-switch value and exhibited a much broader current waveform. These differences will be quantitatively delineated below.

The SIMPLODE code requires as input data the current waveform, mass per unit length, and the inner and outer radius of the plasma slug. The plasma length is taken to be 4 cm in all the calculations presented here. For different lengths the total yield can be appropriately scaled. The selected cases considered are presented in Table 1.

TABLE 1

	$\frac{M}{\ell}$ (μgm/cm)	R_B(cm)	R_i(cm)
	23.5	1.45	1.05
	23.5	1.55	0.55
No-Switch	23.5	1.786	0.655
	25.0	1.55	0.95
	35.0	1.55	0.95
	.23.5	1.45	1.05
Switch	23.5	1.55	0.95
	23.5	1.786	0.655
	35.0	1.55	0.95

The experimental current waveform for the no-switch cases is shown in Fig. 1. The current reaches a peak value of 1.25 MA, has a current risetime of about 40 ns, and a FWHM of 90 ns. The measured current waveform as recorded by the current monitors crowbars at about 130 ns and maintains a steady constant value. In reality, the current vanishes at late time. We have taken the liberty of extending it to zero at 135 ns to insure that it does vanish. This current waveform has been used for all the no-switch simulations. This is strictly not correct since the load impedance varies in time and this is not reflected in a modified current trace. In the future, SIMPLODE will be coupled to a circuit model that uses the open circuit voltage to self-consistently predict a current for a time varying load. As an example of the no-switch case we present the results of the SIMPLODE code for the current trace shown in Fig. 1 and the initial conditions: M/ℓ = 30 μgm/cm, R_o=1.55 cm and R_i=0.95 cm. Figure 2 shows the time evolution of the inner and outer radius. Note that the outer radius pinches down to about 0.5 mm and bounces back out at 150 ns, i.e., the fluid pressure exceeds the magnetic pressure and pushes the plasma out. This happens significantly after peak current. The implosion velocity of the

outer surface is shown in Fig. 3 and reaches a maximum value of 2.1 cm/μsec and is zero at the bounce time. The effective charge state, ZEFF, is shown in Fig. 4 and is merely a reflection of the temperature and density of the plasma. The sharp spikes are not real but are numerical artifacts associated with the time-step used in this particular calculation. If a significantly smaller time-step was used these artifacts would disappear leaving a smooth curve. However, reduction in Δt leads to significant increases in computer time. Test runs with smaller Δt's produce values equivalent to "eyeball" averaging and smoothing of the results presented in Fig. 4. The effective charge state of the plasma is about 8 at 50 ns. The temperature is shown in Fig. 5 and reaches a peak value of about 125 eV around 140 ns. This occurs well after peak current and during the final compression phase before bouncing out. The ion density peaks around 150 ns with a value of 2.2×10^{20} cm^{-3} as shown in Fig. 6. Both temperature and density peak during the final compressional phase. The ion density has a narrow, well peaked delta-function like profile representative of a good compressional implosion. The local K-shell radiative yield is shown as a function of time in Fig. 7. A sharp pulse is emitted over 12 ns beginning at about 135 ns and essentially terminating around 147 ns attaining a peak value at 145 ns. Finally, the total integrated K-shell yield is shown in Fig. 8. The total K-shell yield is about 2.1 kj and is approximately the same as the majority of GAMBLE II results. Maximum K-shell yield for GAMBLE II neon experiments is predicted to be about 4 kj. This optimized yield has been achieved experimentally.[6]

A similar set of numerical simulations were carried out for the case of the PEOS. The initial mass per unit length and radii are the same as the case above. However, as already noted the current trace is different. With the PEOS the current waveform is represented by the profile shown in Fig. 9. The peak current is about 0.88 MA, sharper current risetime and a broader profile width. The current also remains on for a longer period of time - until around 220 ns - a full 85 ns longer than the no-switch

case. The details of the implosion dynamics are shown in Figs. 10-16. Note that with reduced peak current it takes longer to drive the plasma in and results in a somewhat softer compression. This is reflected by the slower implosion velocity and corresponding cooler temperatures and lower densities leading to reduced K-shell yields. These results indicate that peak current and its maintainence appear to be the only parameters that influence significantly the yield, assuming some optimization of the kinematics. The influence of the current risetime will be discussed below. This revelation is not surprising and is consistent with our earlier findings[4] and is in agreement with most 0-D codes.

We will now discuss the results of a series of numerical simulations illustrating the systematic behavior of the kinematic variables and yield as a function of mass and radius. The first series of simulations varies the mass/length while maintaining the initial radii fixed, i.e., R_o = 1.55 cm and R_i = 0.95 cm and M/ℓ varies between 15 to 35 μgm/cm in 5 μgm/cm steps. Figure 17 shows the maximum velocity as a function M/ℓ for both the switch and no-switch cases. For a fixed peak current, the higher the M/ℓ the smaller the peak velocity of implosion-pushing on the plasma with a greater magnetic force produces a greater plasma acceleration. These results suggest the following scenario: the higher the peak current the higher the peak temperature, density, and K-shell yield, provided, of course, that the current is not so high that it burns through the K-shell, which would result in a reduced K-shell yield. This is shown in Figs. 18-20 which compares the switch and no-switch results. The higher the peak current the better the quality of the implosion, assuming optimized kinematics, again provided there is sufficient mass for good K-shell emission. The neon K-shell yield presented in Fig. 20 shows that below about 22 μgm/cm the K-shell yield is actually greater for the lower peak current (switch) case than the no-switch case. The explanation is that the higher current no-switch case burns through much of the K-shell for low mass loads and hence, has fewer K-shell emitters and therefore produces a

reduced yield. Above 22 μgm/cm the no-switch yield continues to increase as the available number of K-shell emitters increases. Also note that in support of this behavior the yields of each case is optimum for different masses: the no-switch case at about 26 μgm/cm and the PEOS case at about 22 μgm/cm. The percent ratio in peak current is virtually the ratio of yields; i.e., peak currents are in the ratio of 8/12.5 = 64% while the peak K-shell yields are in the ratio of 2.1/3.2 = 65%. This is not meant to suggest that the relationship between current and yield is a linear one, because it is *not*, it is only indicative that in general, for optimum kinematics, the higher yields are associated with higher currents. In fact, a scaling law has been derived and suggests that the K-shell yield scales approximately as the fourth power of the peak current (actually $I^{3.8}$).

The influence of current risetime on the yield is not as obvious from these calculations as it is from the experiments. The experiments indicate a sharper risetime current profile, and larger yield of the radiation K-shell pulse when the PEOS is used. Also, the plasma appears to exhibit less flaring and more uniformity with the PEOS. Calculationally, we cannot comment on the plasma structure with the 0-D code but the 0-D results predict good yields. In fact, a series of runs were made with a reduced peak current in the no-switch case equal to the peak current in the PEOS case. The yield was half the PEOS yields supporting the notion that sharper current risetime's influence the yield. It's as if the current "hits" the load so quickly that the load just percolates and then coasts inward producing a more uniform implosion. Obviously this is an area that requires further investigation if we are to understand the influence of sharp current risetime pulses on the implosion processes.

The final set of numerical simulations involves keeping the mass per unit length fixed while varying the initial sheath thickness. The conditions are for M/ℓ=30μgm/cm and a fixed outer radius of 1.55 cm. The results of the calculations are shown in Figs. 21-24 for both current cases. The peak velocities decrease

slightly with increasing Δr which just reflects the behavior of the outer boundary vis a vis the inner boundary: i.e., since the mass, outer radius, and current are fixed the only variable parameter is the inner radius. Depending on the time it takes the inner radius to collapse influences the competition between magnetic and fluid pressure and the bounce time of the outer boundary. In Fig. 22 the peak densities are plotted as a function of Δr. The higher densities occur for lower values of Δr and result from more particles per unit volume initially (even though the total number of particles per gram is the same in all cases) combined with a better implosion, i.e., higher velocity and greater compression. For larger Δr the difference between the switch and no-switch cases is not readily discernable on the graph but the no-switch case is about a factor of two greater for the higher values of Δr. The peak temperatures as a function of Δr are shown in Fig. 23. At first glance the results appear contradictory in the sense that it might be anticipated that the temperature would decrease as the sheath thickness increased since the implosion exhibited slower peak velocities and lower peak densities. Actually, the peak temperatures increase because there are fewer emitters which reduces the major source of radiation cooling - line radiation - keeping the plasma hotter. This is further evidenced in Fig. 24 where the peak radiative yields are shown as a function of Δr, i.e., the yield (or alternatively, the radiation cooling) decreases drastically for large Δr. Since the yield is shown only for the K-shell, a logical conclusion is that the temperature becomes hot enough to erode the K-shell, i.e., reduce the number of emitters, and reduce the plasma cooling causing the plasma to remain hot. Finally, the radiation pulses emitted by the plasma experimentally are longer than those calculated. This effect is probably due to the "zippering" effect of the implosion and is not included in the model. Efforts to stagger the implosion to simulate this effect are currently underway.

IV. Summary

A series of numerical simulations were performed to investigate the behavior of an imploding neon gas puff for conditions similar to experiments conducted on the NRL GAMBLE II pulsed power facility. The calculations were done using the SIMPLODE code which is best described as a O-D Non-LTE Dynamic Bennet Pinch model. The Non-LTE model was based on a collisional-radiative equilibrium description in the optically thin approximation. Line radiation from the K-shell only was presented although total radiation was accounted for in the radiative cooling term. The results of the numerical simulations are in reasonably good agreement with the experiments - at least to the extent of the limited comparison. As more experimental data is unfolded, particularly, emission spectra, a more thorough analysis should lead to a better understanding of how to control these implosions. What we have learned from these simulations is that impressive K-shell yields can be obtained with neon on the GAMBLE II facility and that peak current (and possibly current risetime), assuming optimized kinematics, is the single most important parameter in influencing radiative yields.

ACKNOWLEDGMENTS

The authors would like to thank Drs. F. Cochran and R. Terry for helpful discussions. We would also like to thank J. Guillory for paving the way and sharing his experience with us. Also our thanks to F. Young and S. Stephanakis for sharing with us the experimental data and discussing its interpretation.

This work was supported by the Defense Nuclear Agency.

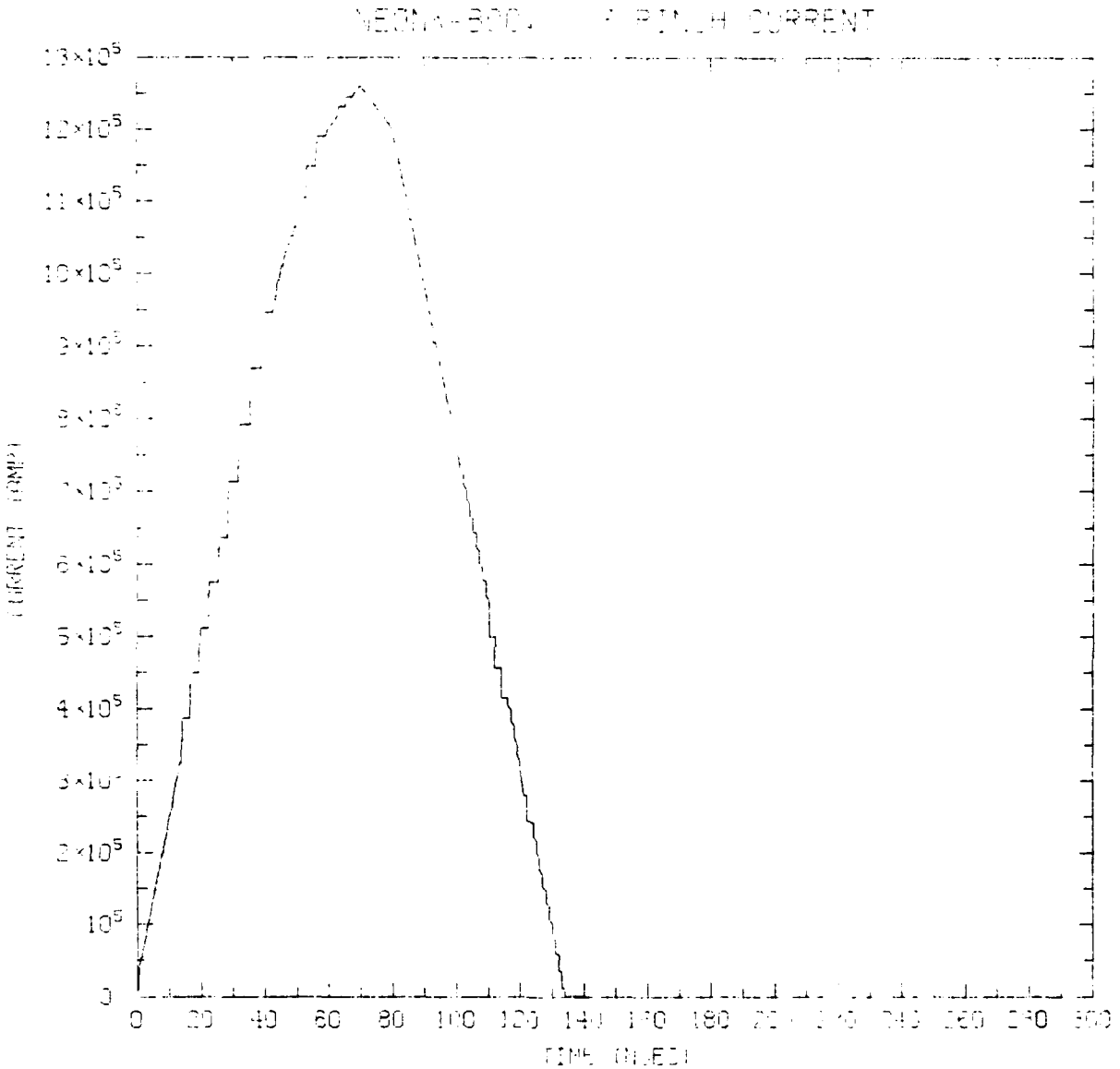

Fig. 1. No-Switch Current vs Time.

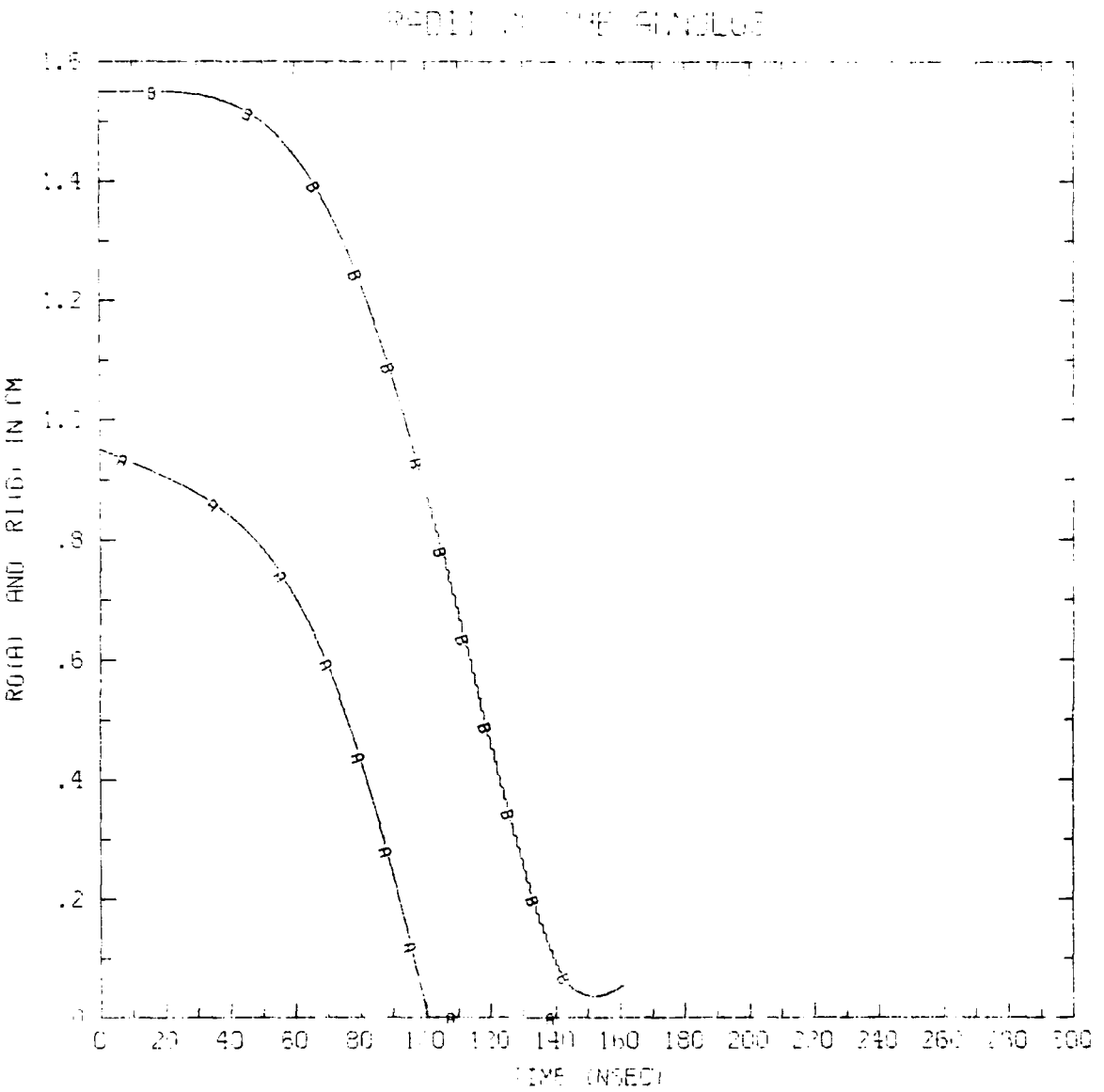

Fig. 2. Radius vs Time.

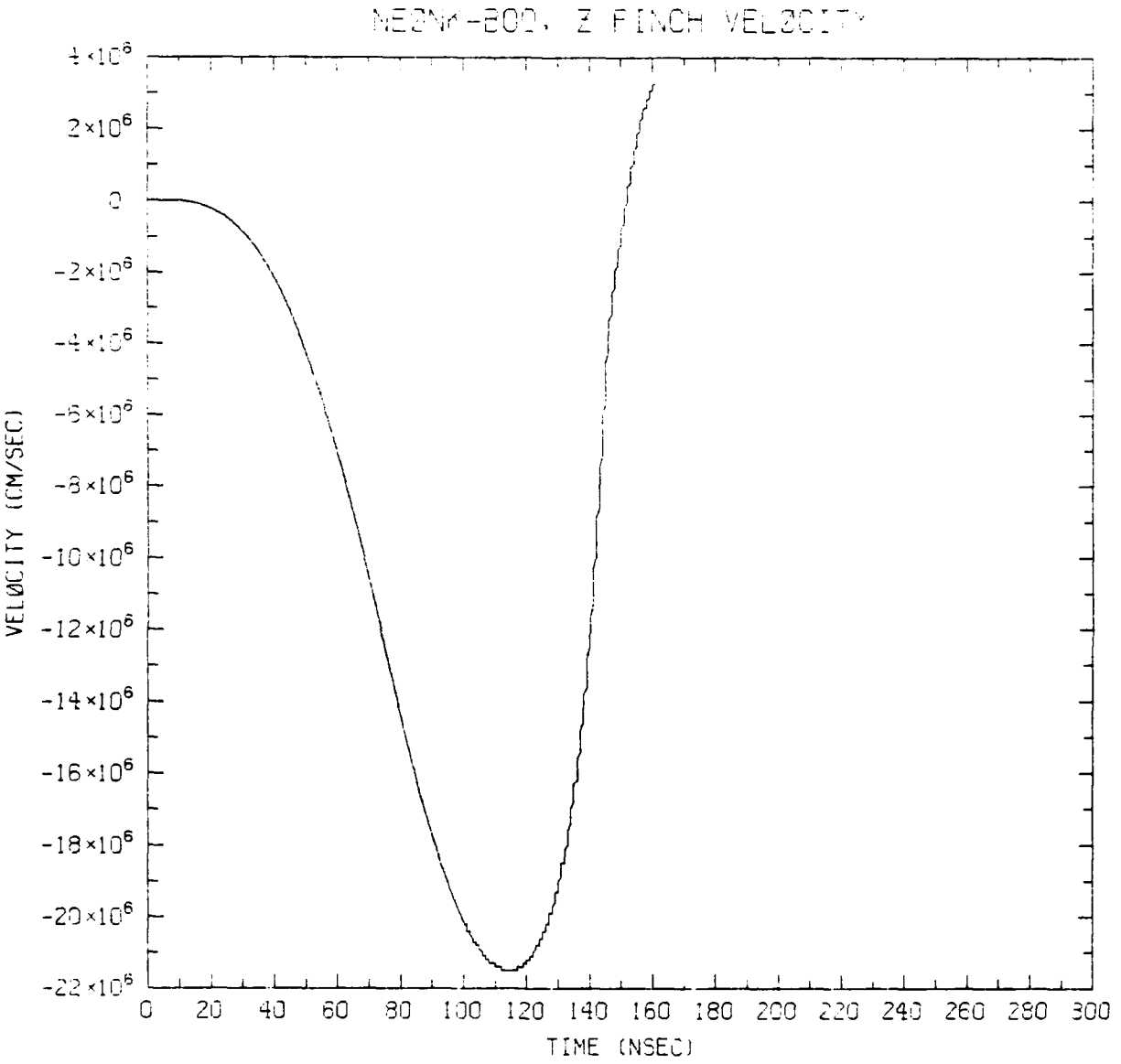

Fig. 3. Velocity vs Time.

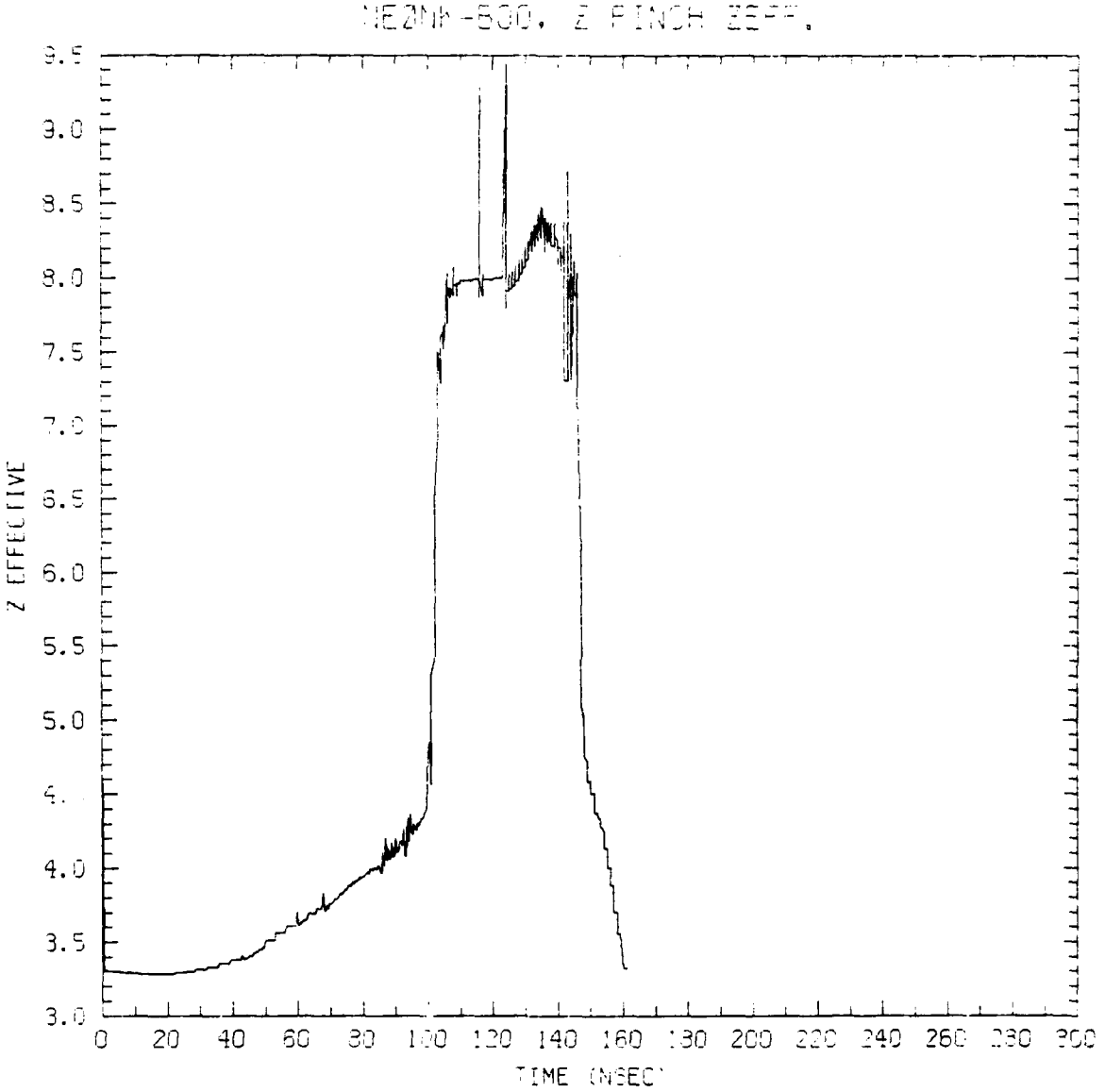

Fig. 4. Effective Charge State vs Time.

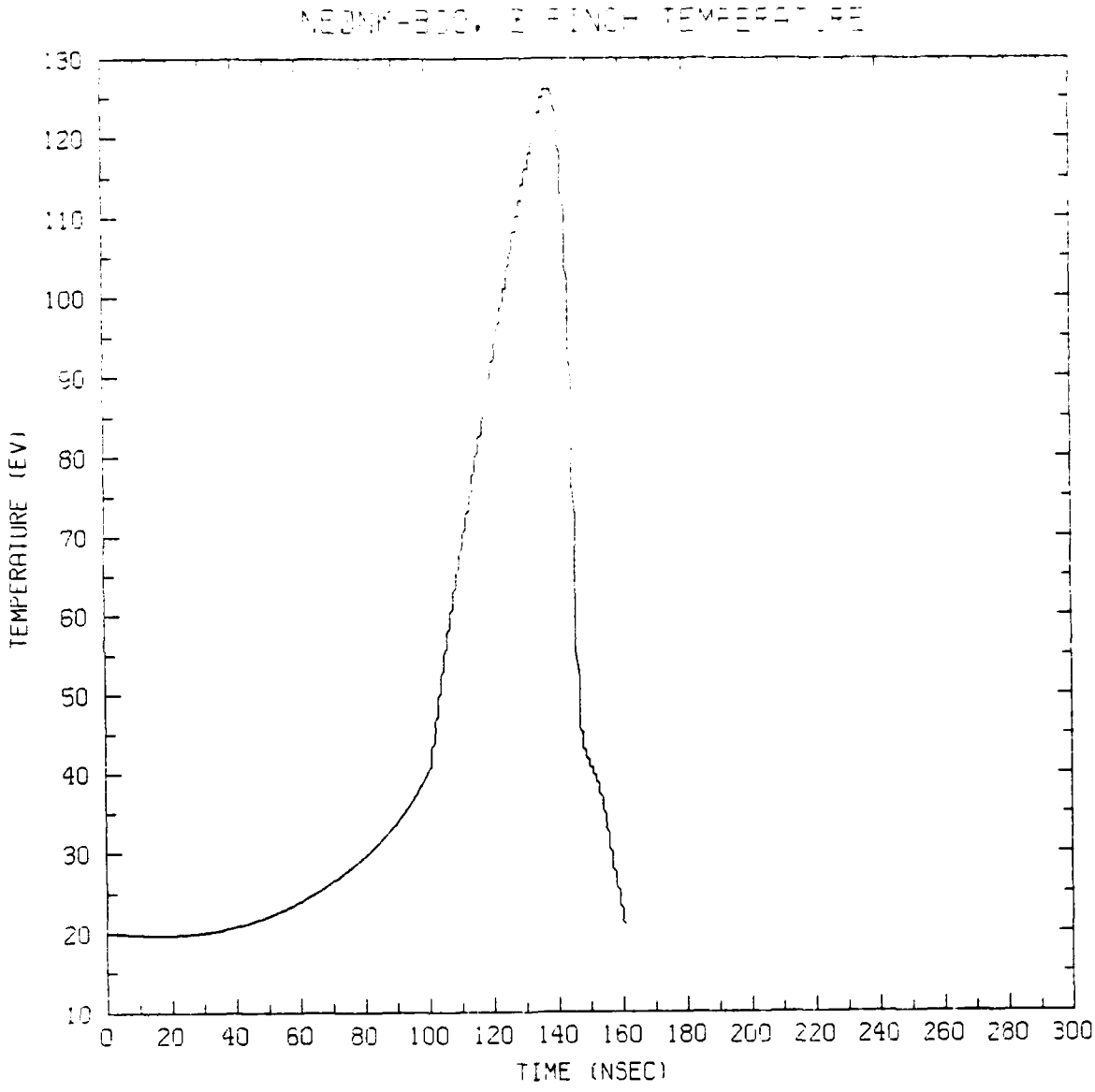

Fig. 5. Temperature vs Time.

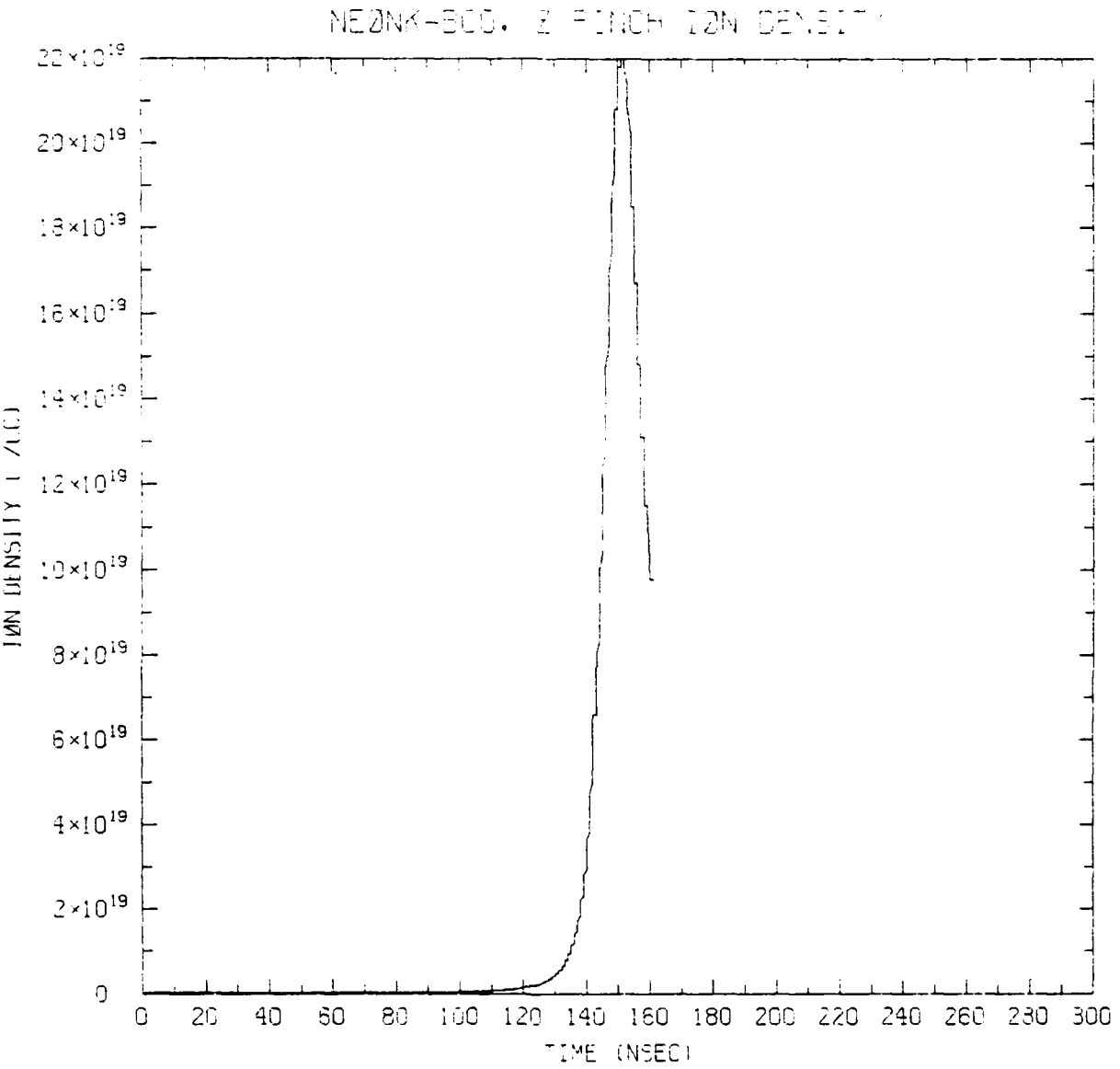

Fig. 6. Ion Density vs Time.

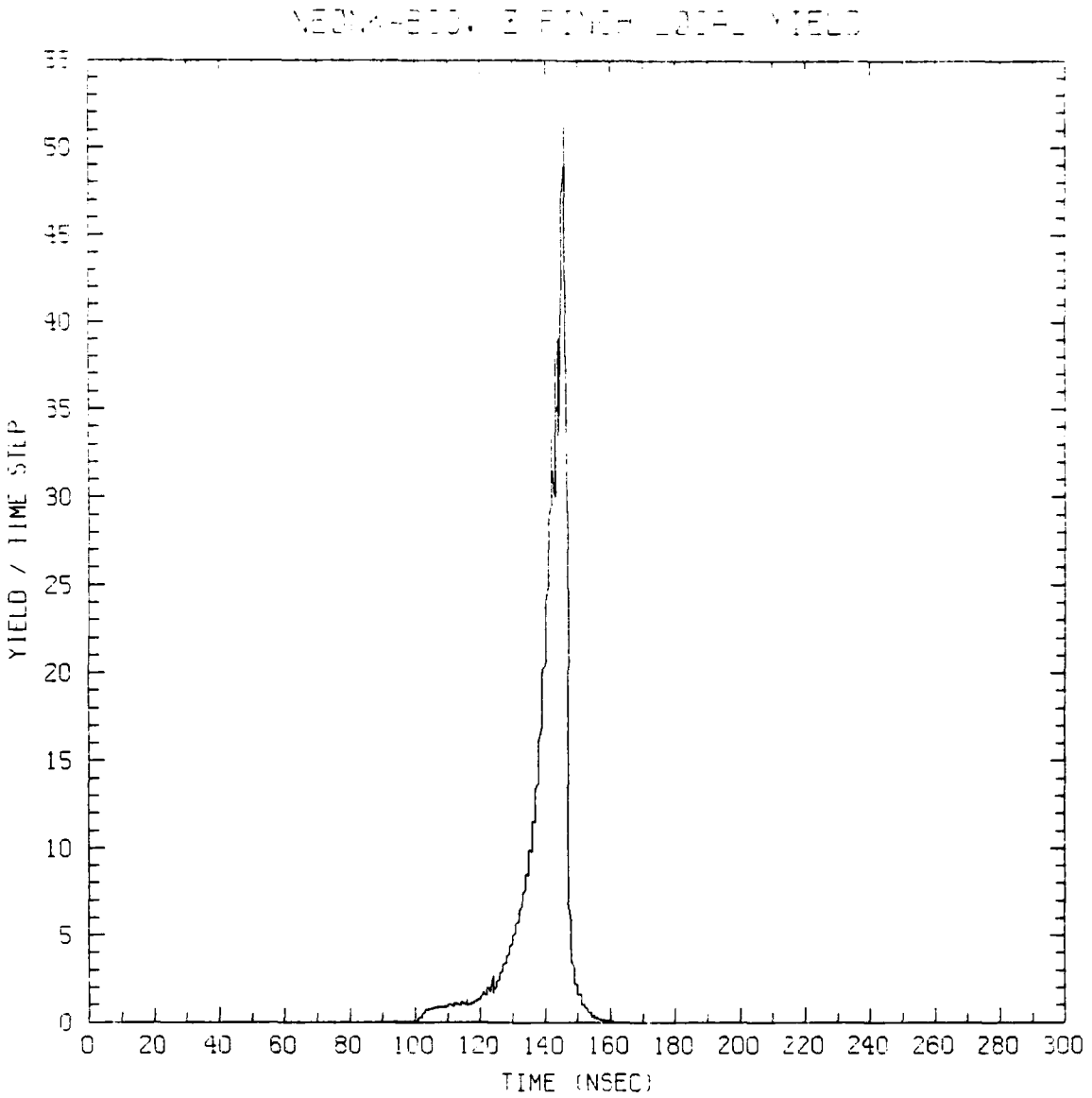

Fig. 7. Local Yield vs Time.

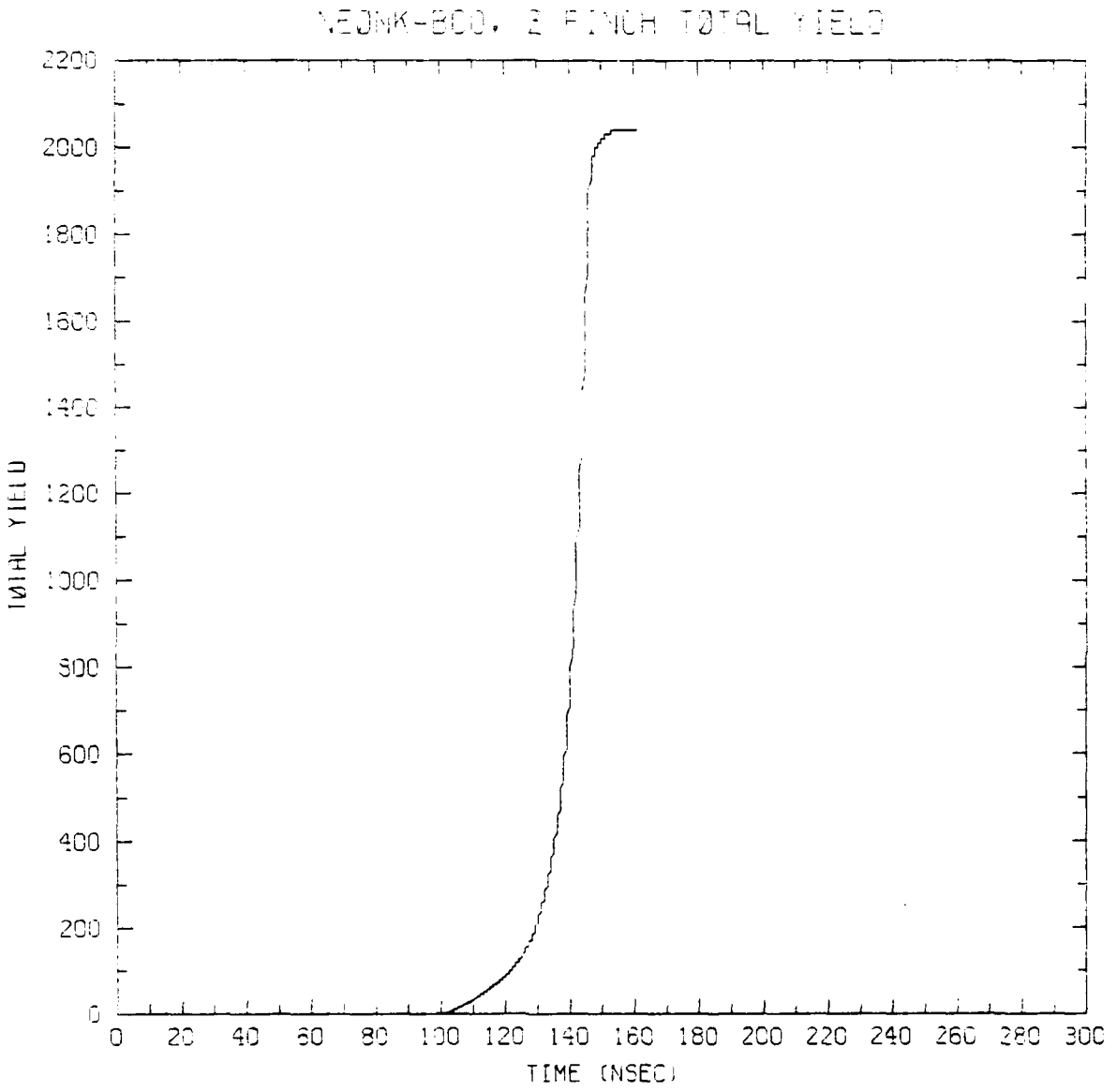

Fig. 8. Total Yield vs Time.

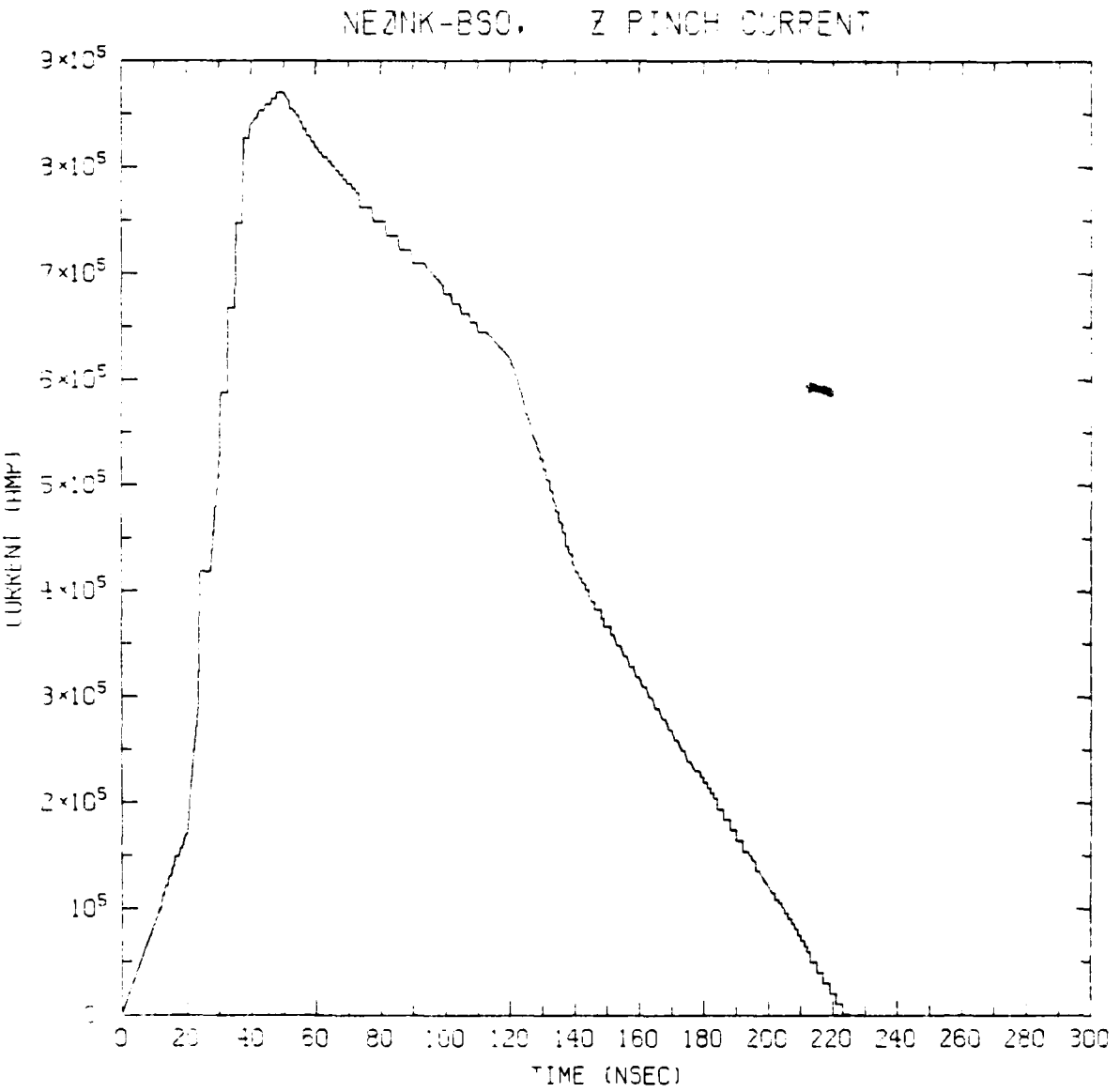

Fig. 9. PEOS Current vs Time.

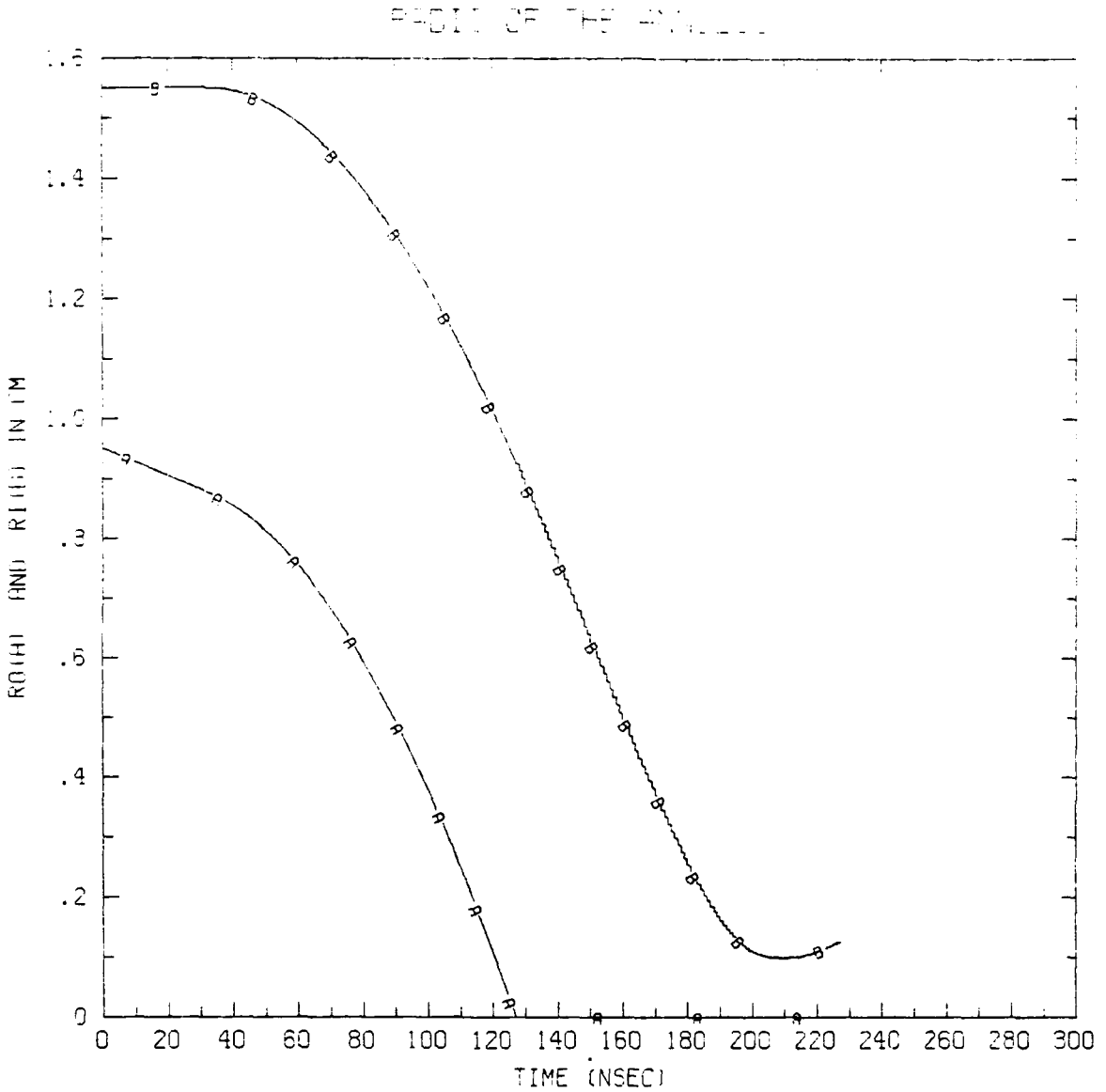

Fig. 10. Radius vs Time.

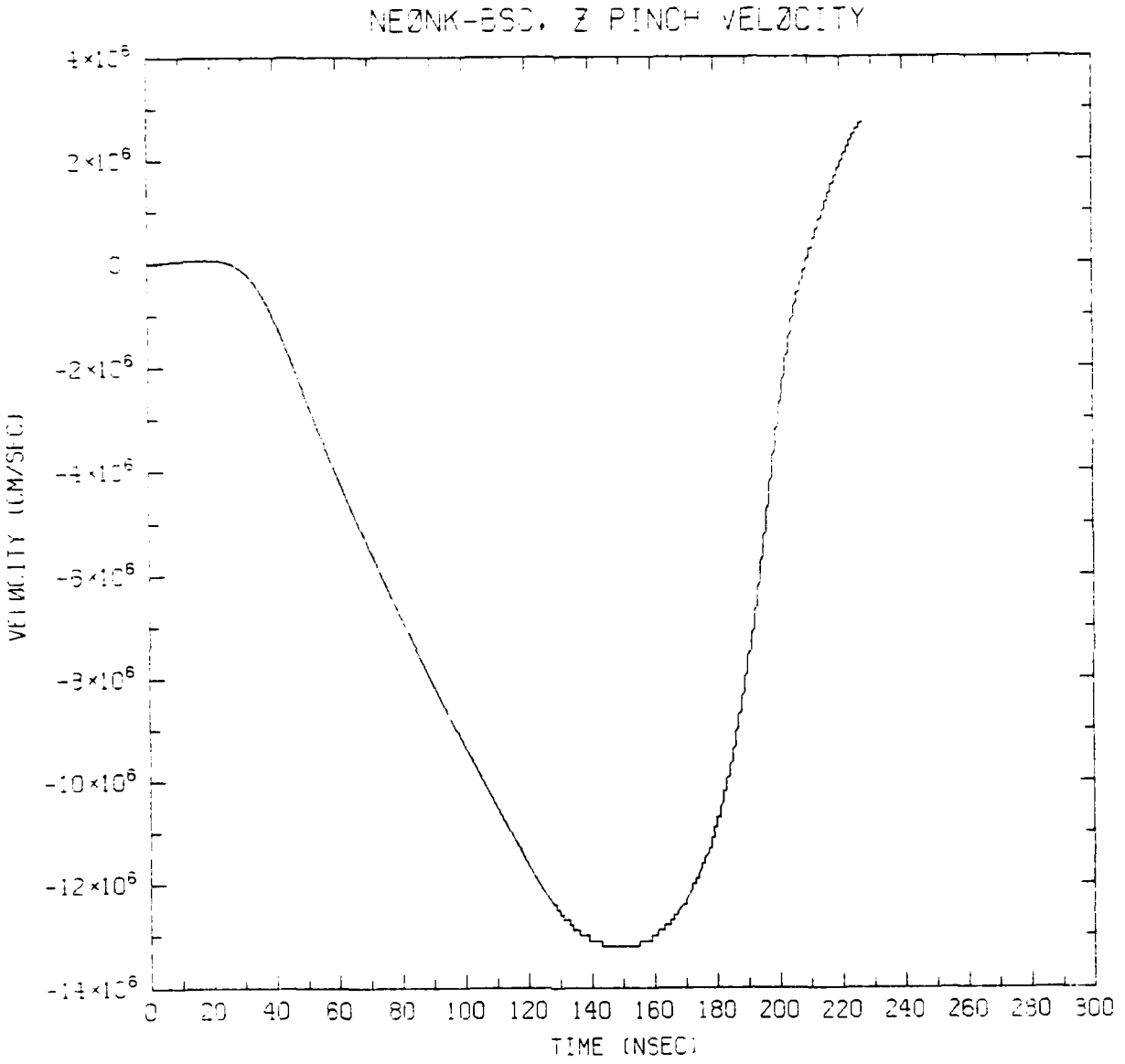

Fig. 11. Velocity vs Time.

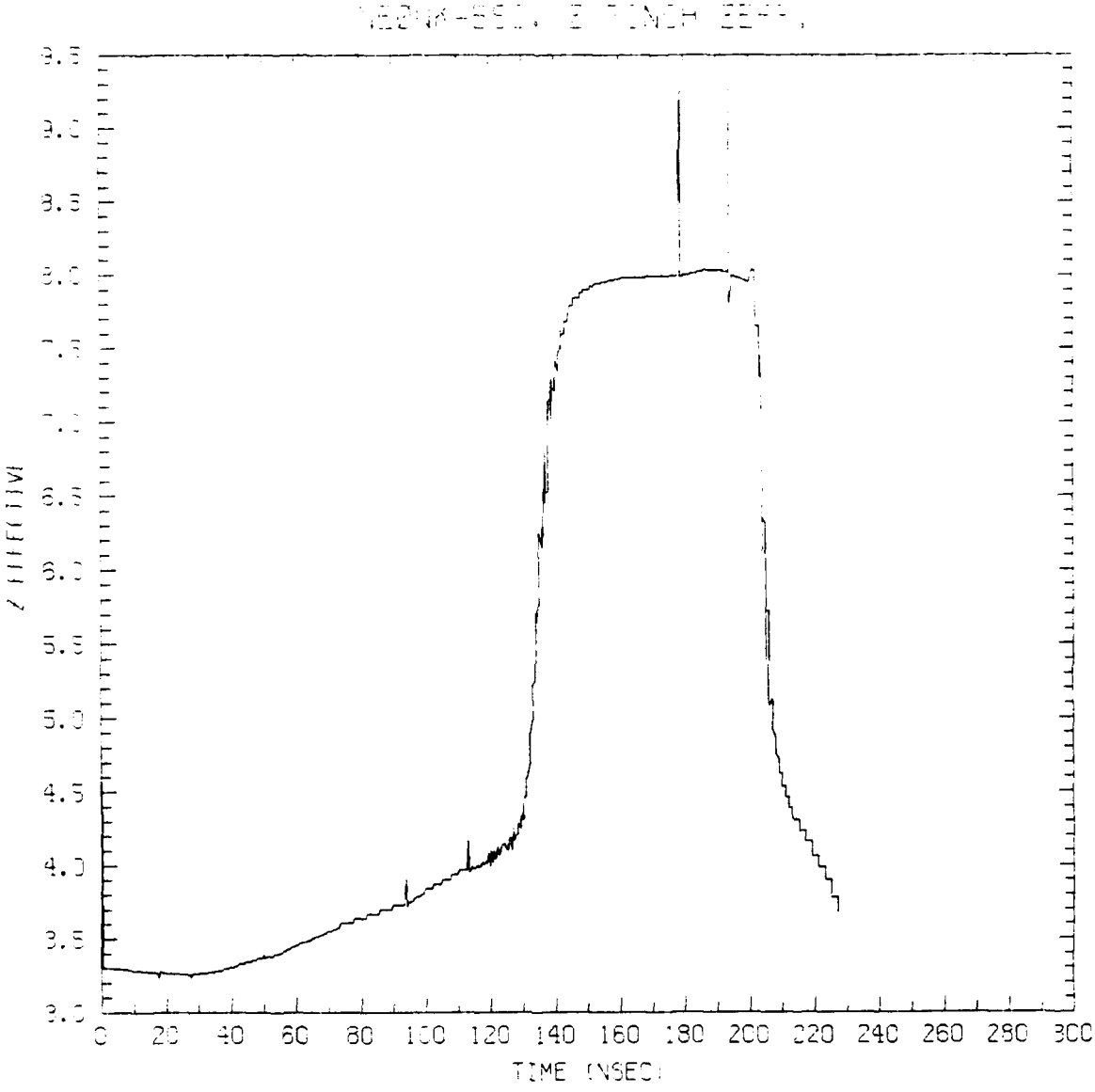

Fig. 12. Effective Charge State vs Time.

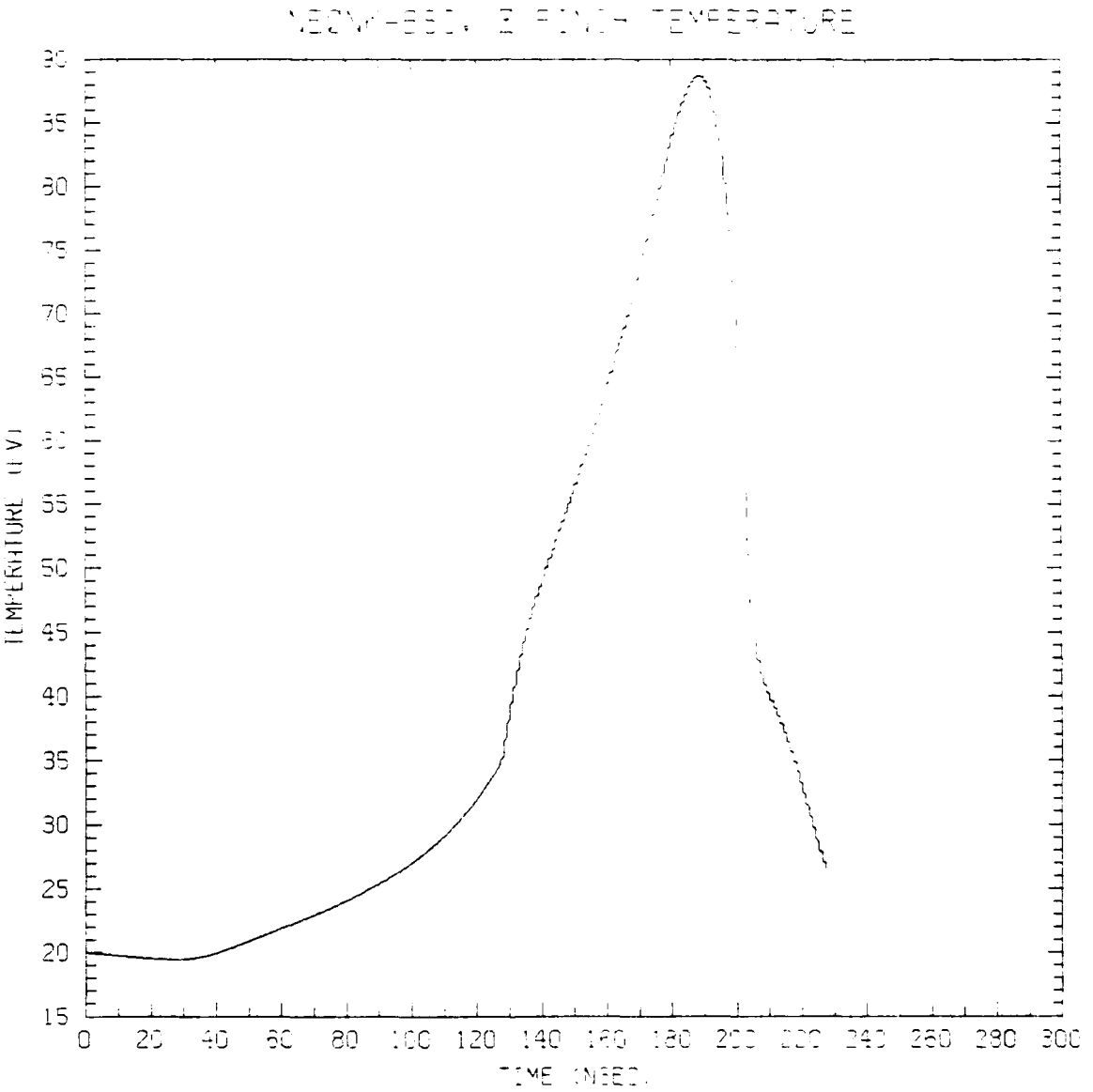

Fig. 13. Temperature vs Time.

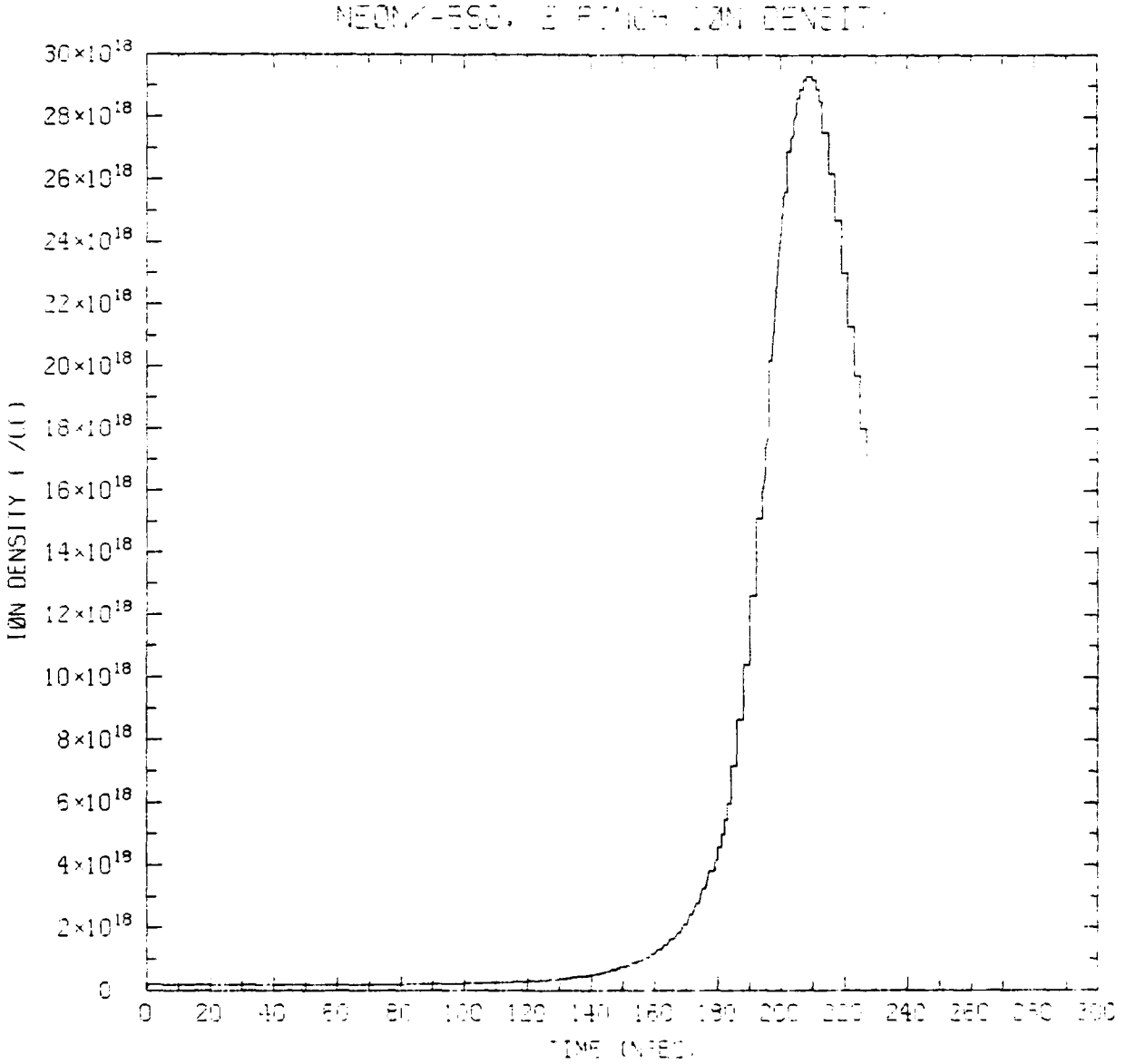

Fig. 14. Ion Density vs Time.

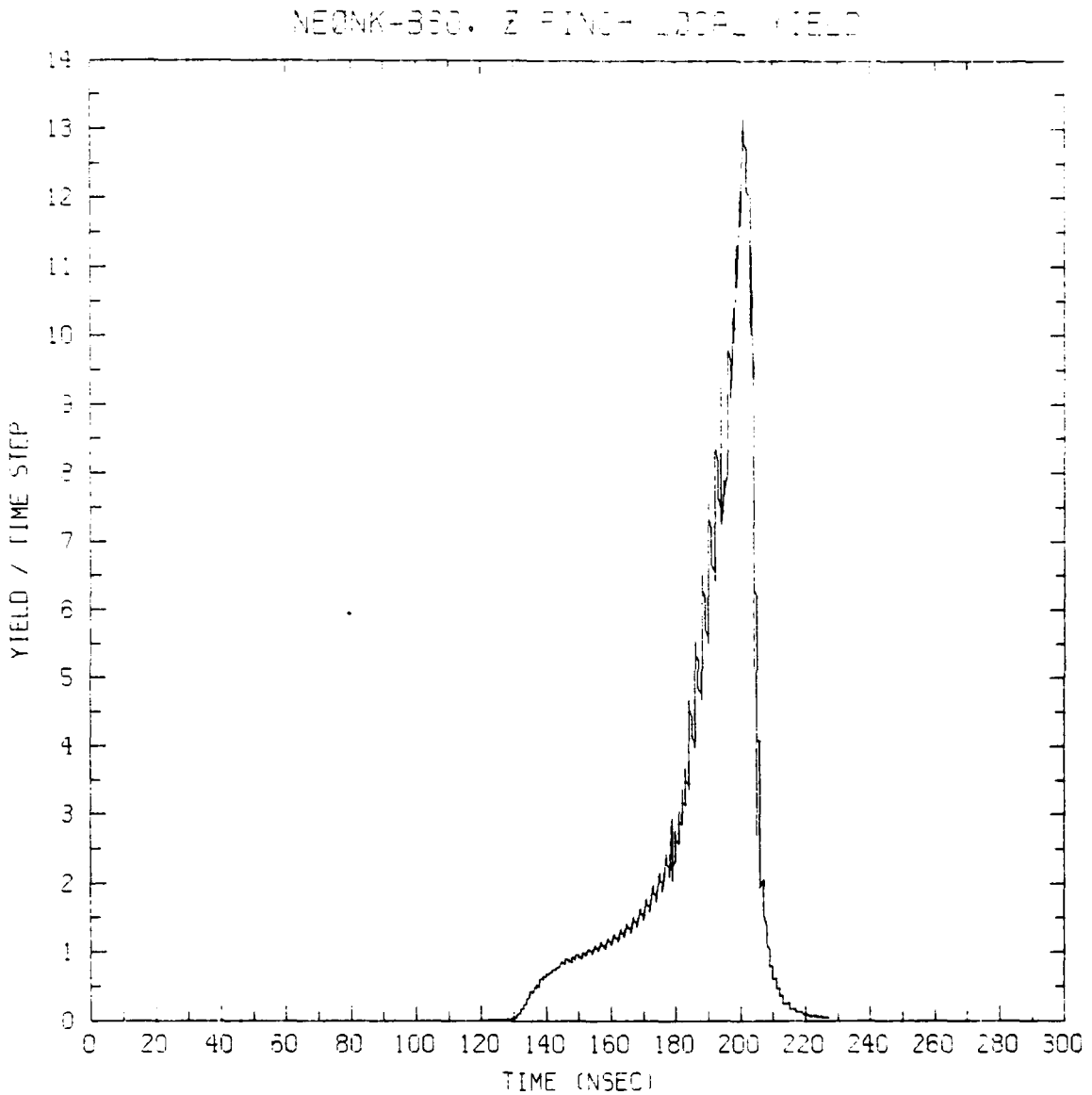

Fig. 15. Local Yield vs Time.

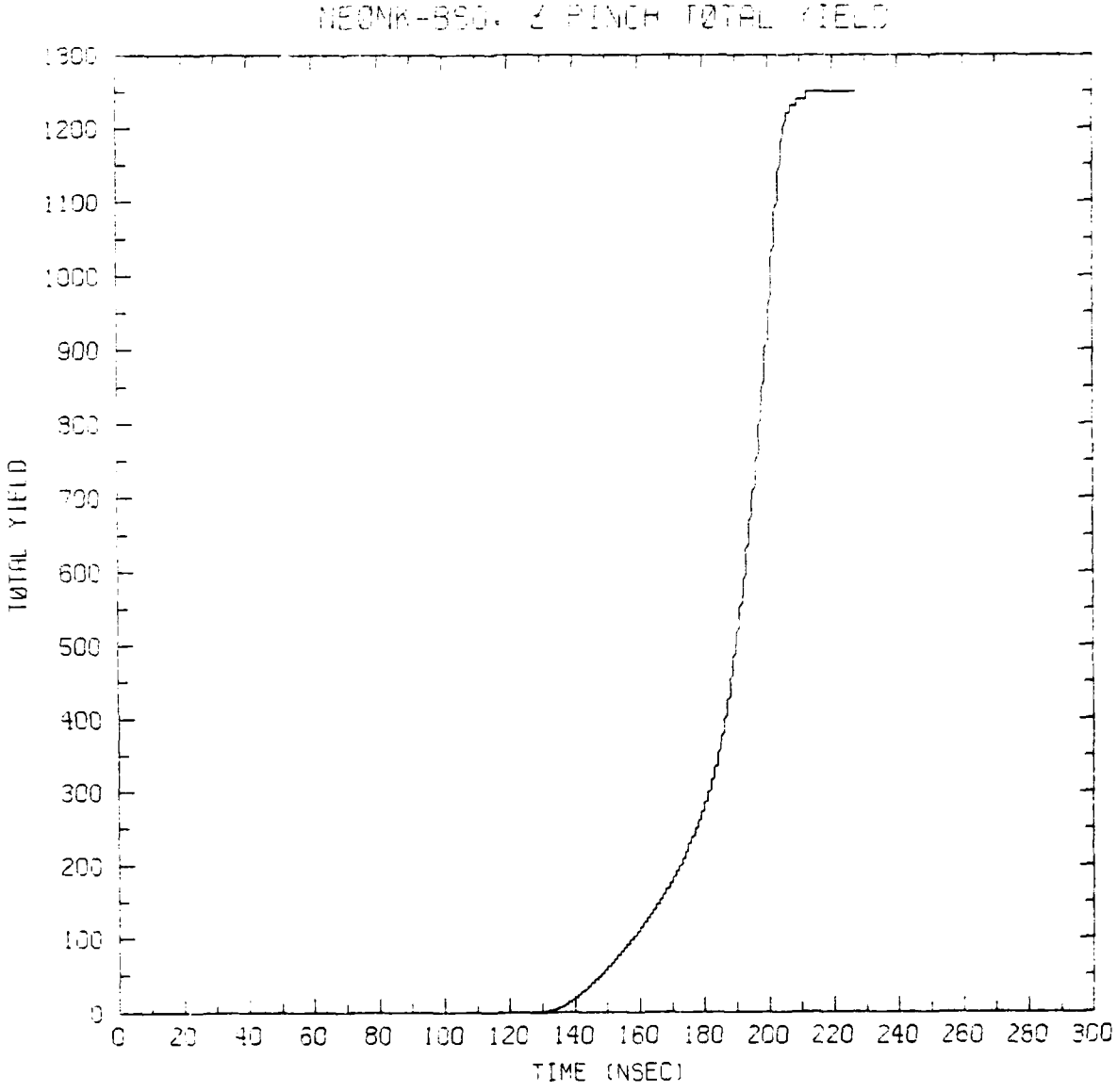

Fig. 16. Total Yield vs Time.

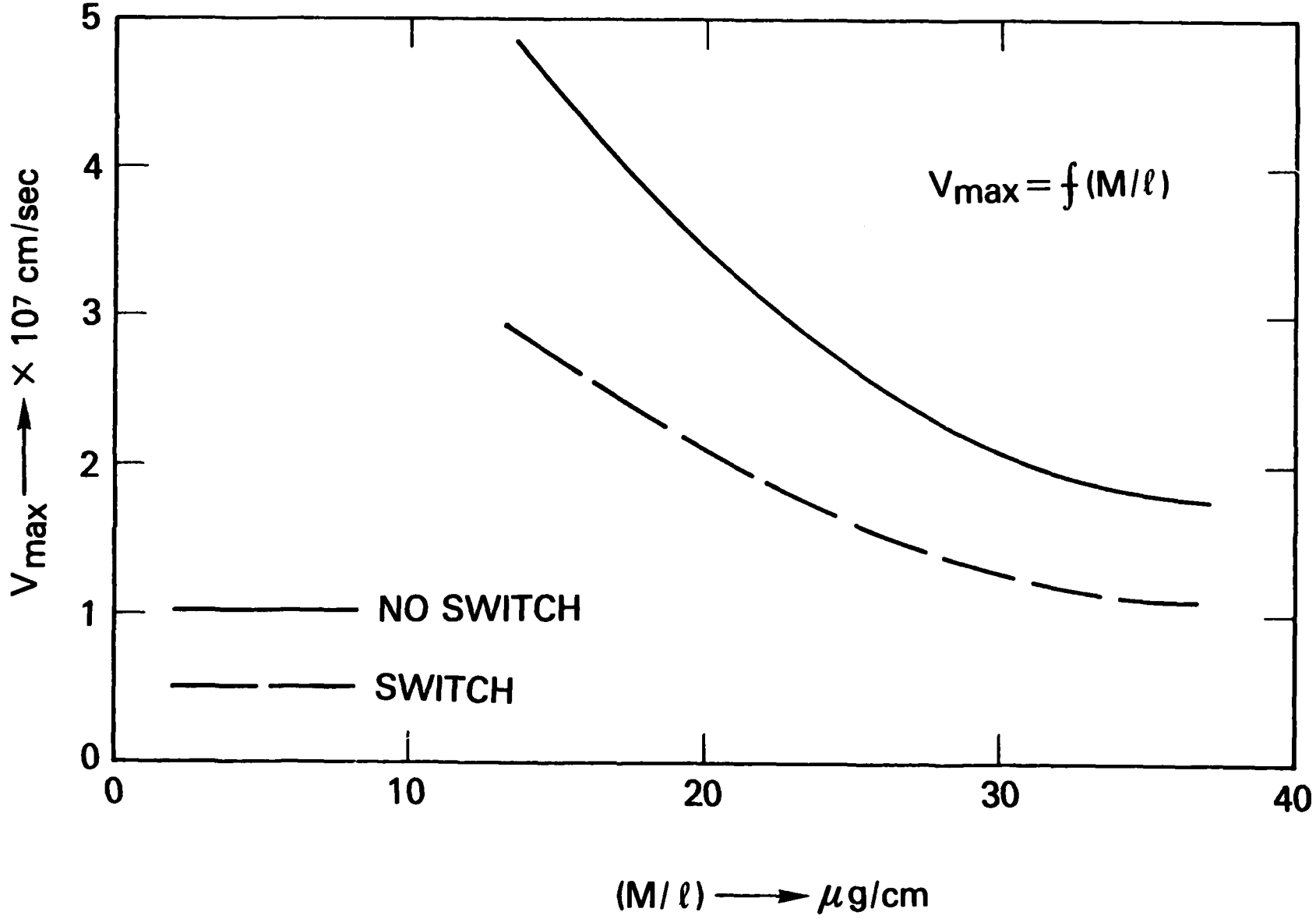

Fig. 17. Maximum Velocity vs Mass for Fixed Radius.

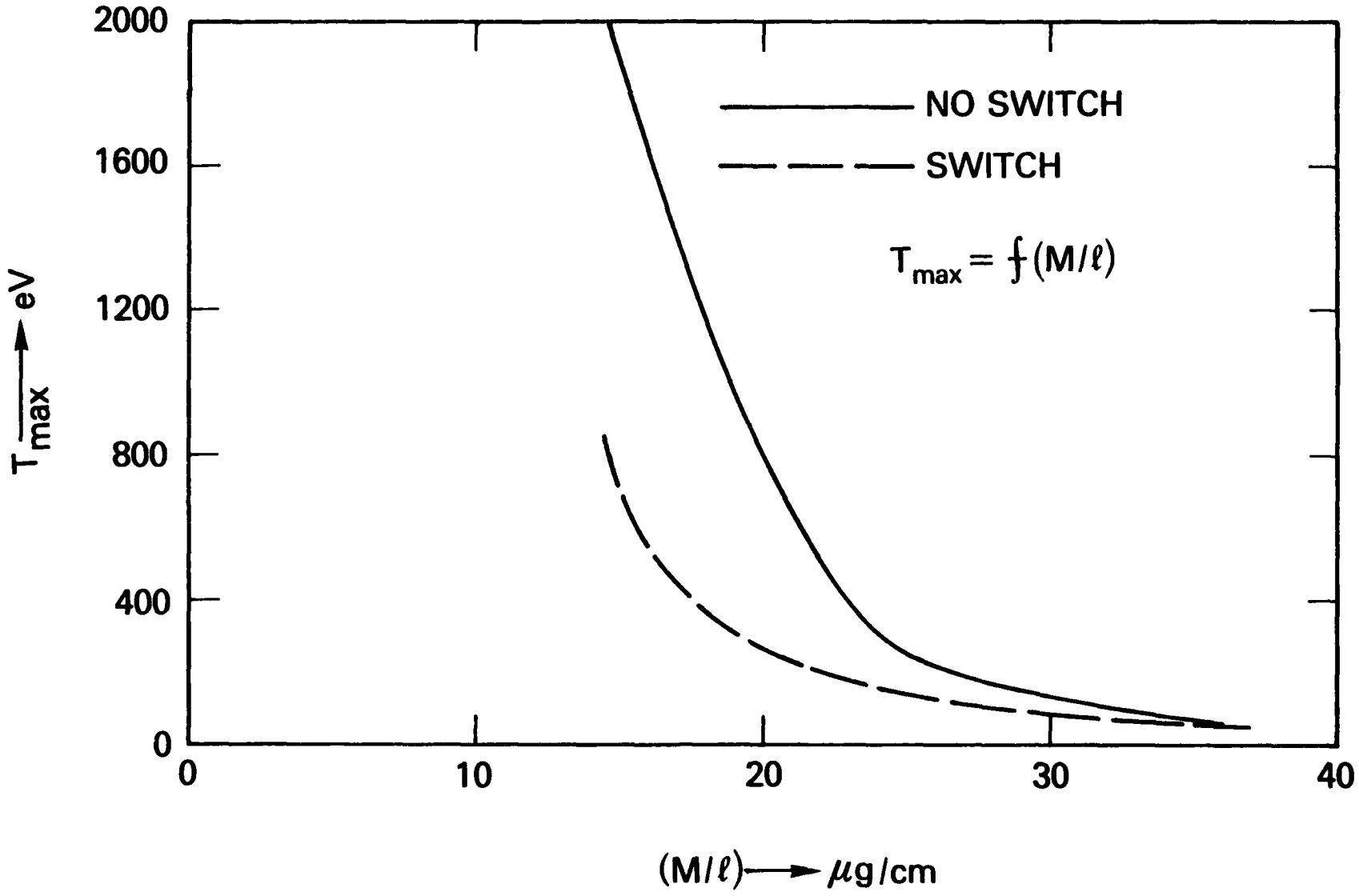

Fig. 18. Maximum Temperature vs Mass for Fixed Radius.

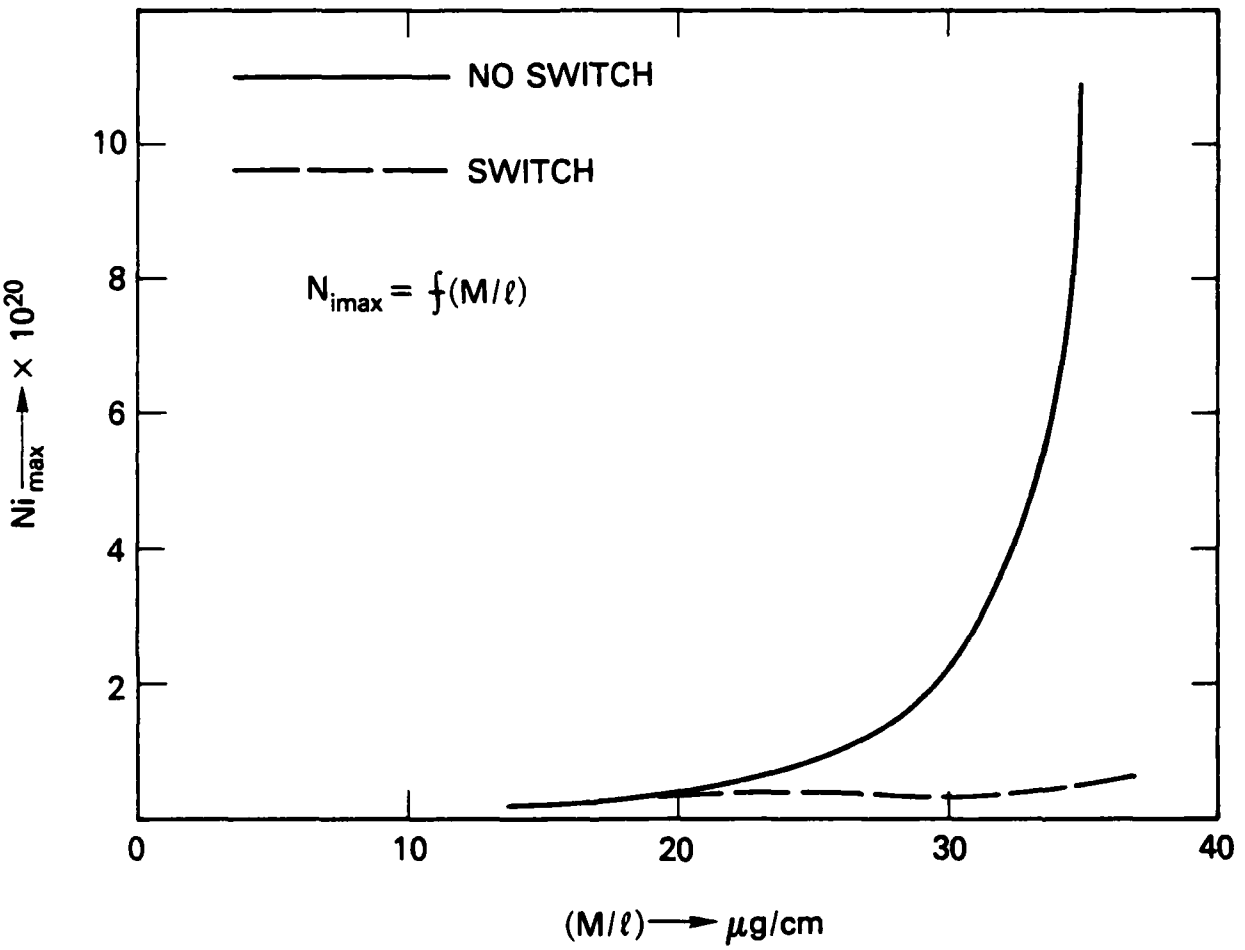

Fig. 19. Maximum Ion Densities vs Mass for Fixed Radius.

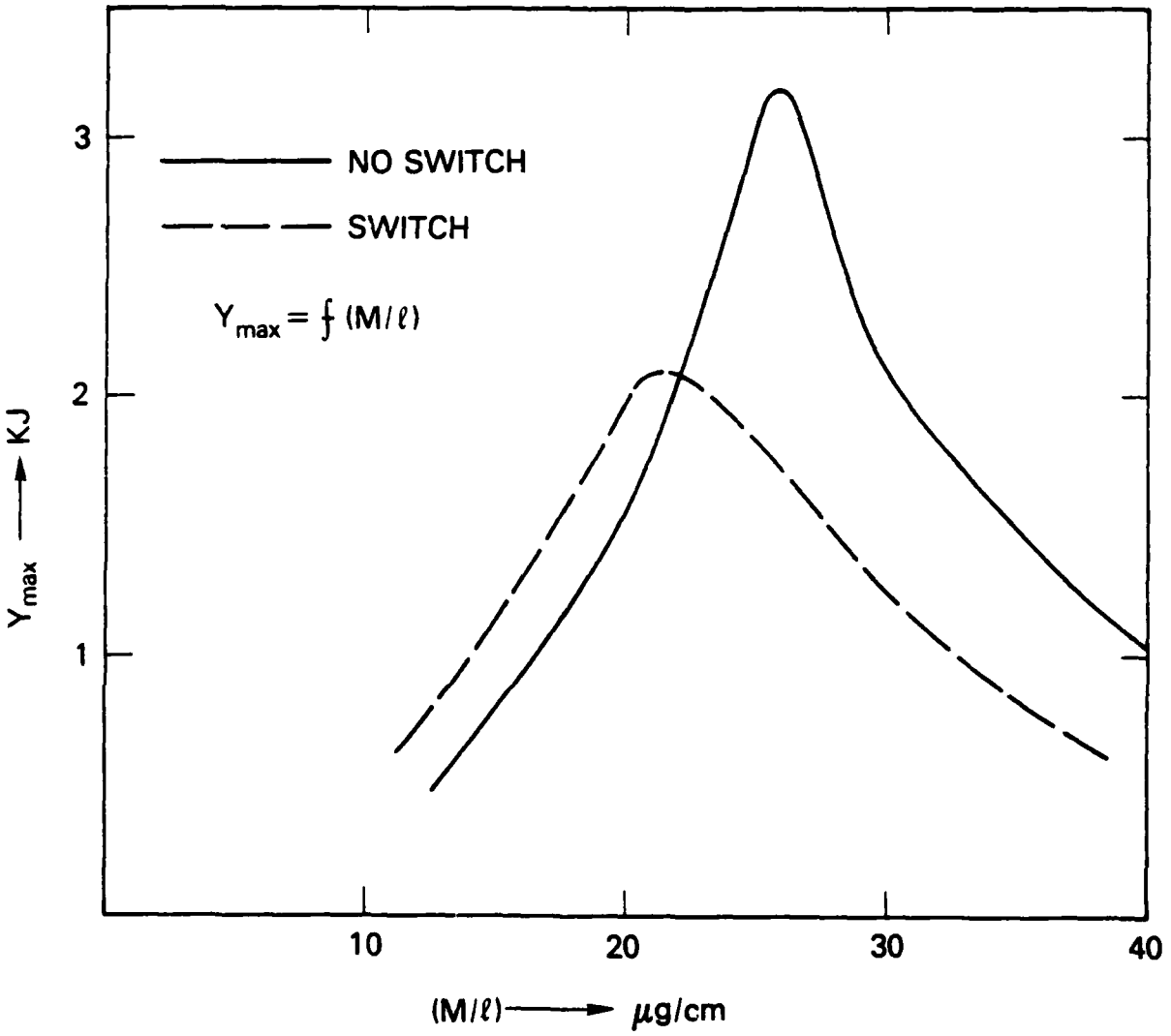

Fig. 20. Maximum Yield vs Mass for Fixed Radius.

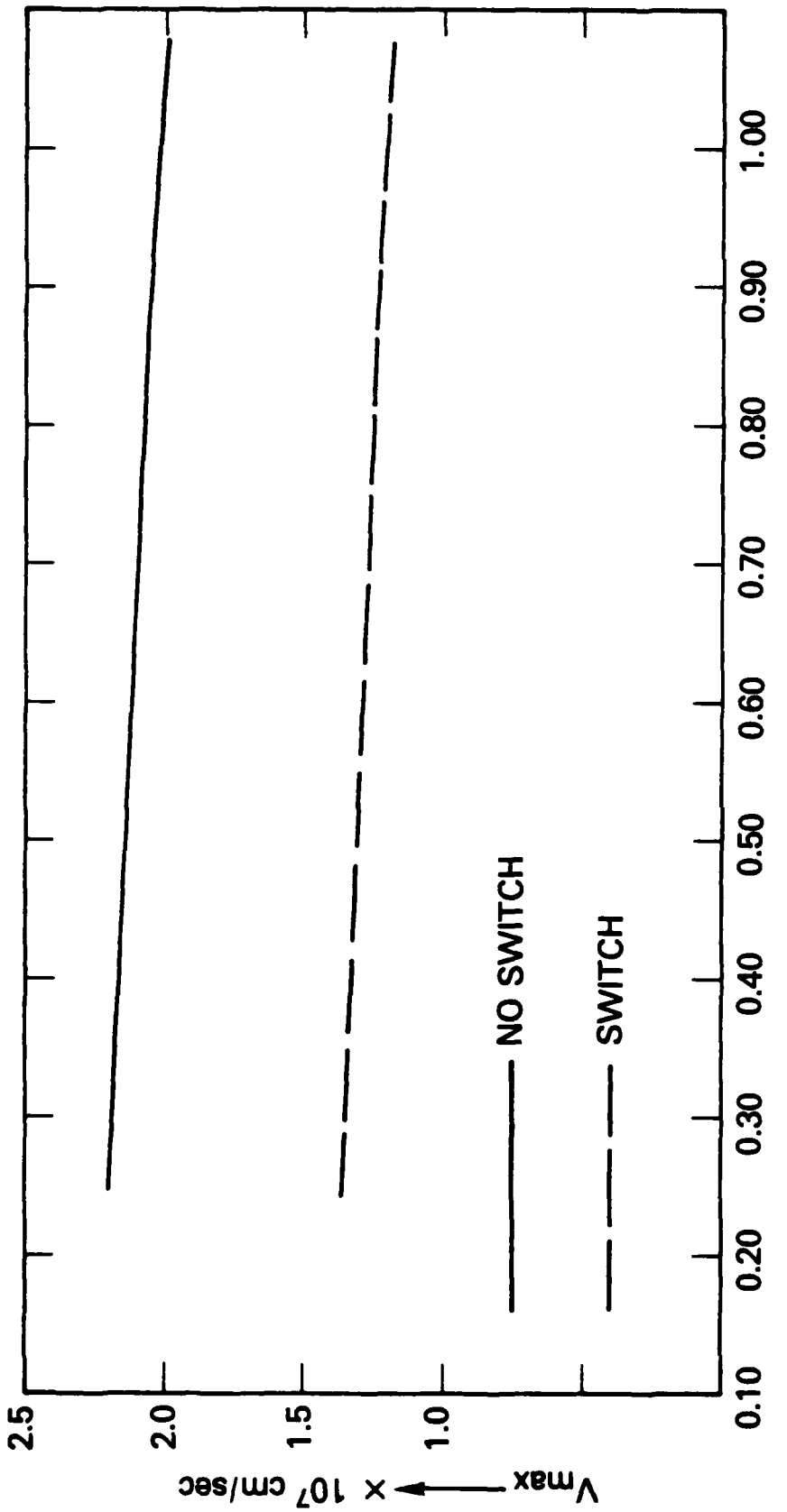

Fig. 21. Maximum Velocity vs Shell Thickness for Fixed Mass.

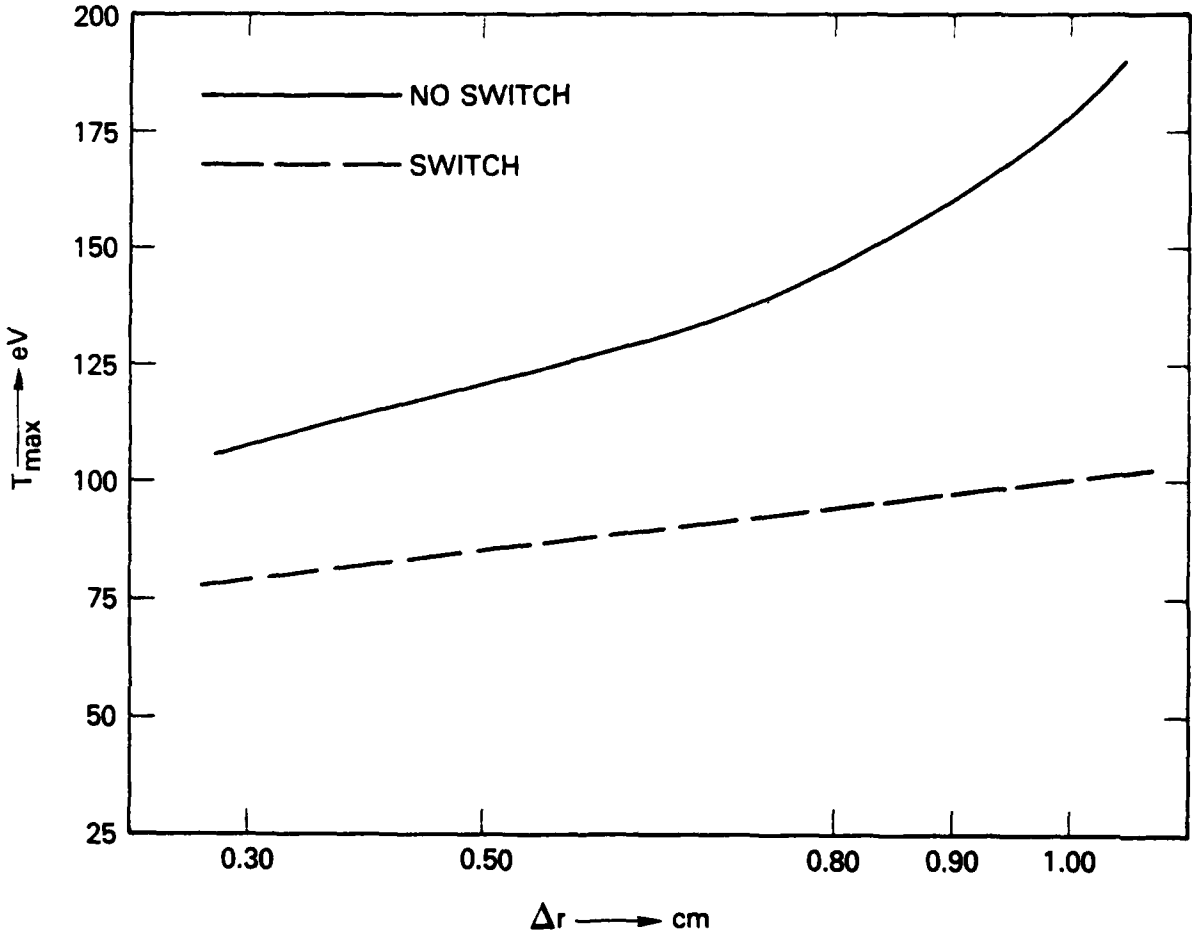

Fig. 22. Maximum Temperature vs Shell Thickness for Fixed Mass.

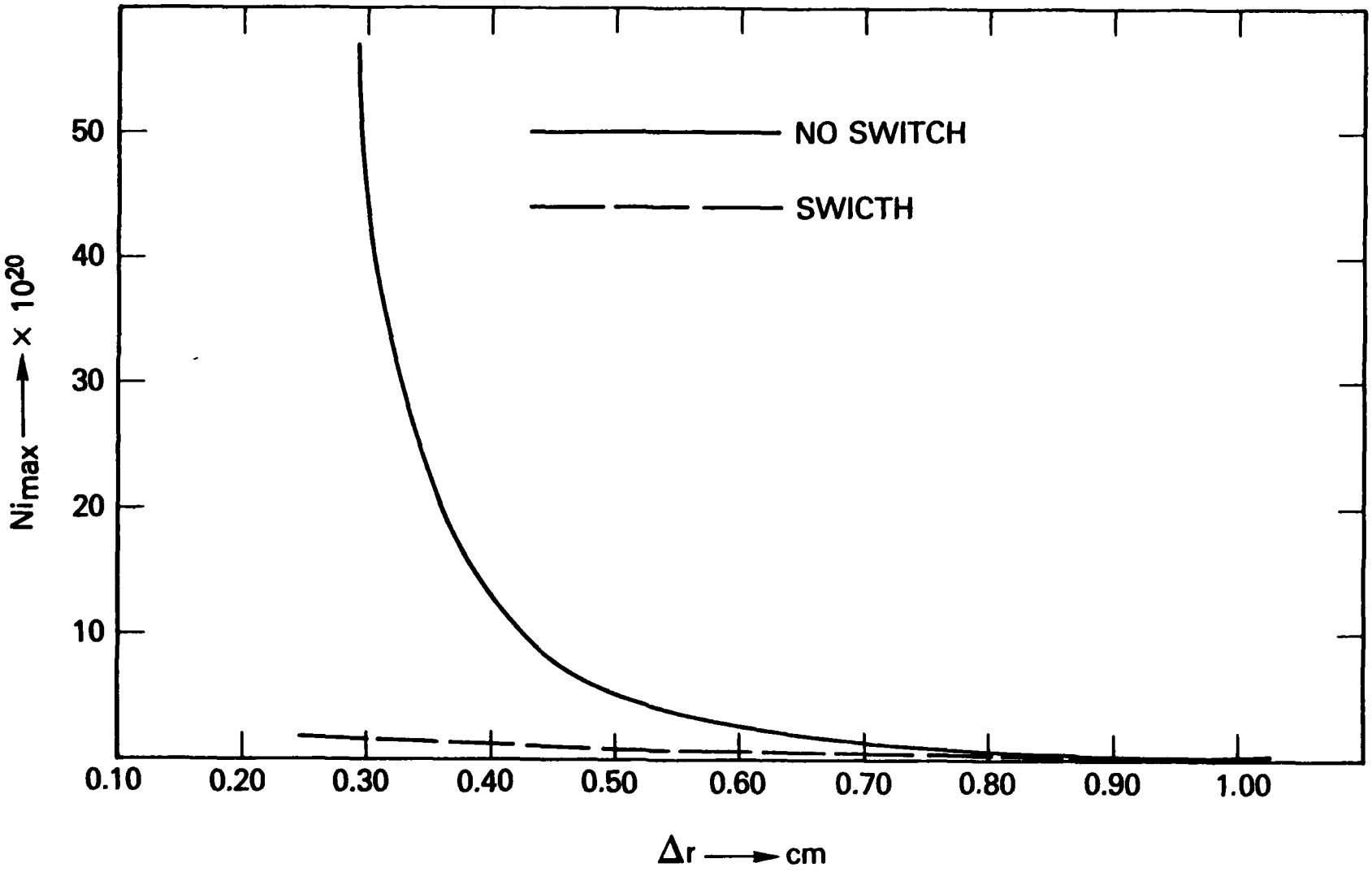

Fig. 23. Maximum Ion Density vs Shell Thickness for Fixed Mass.

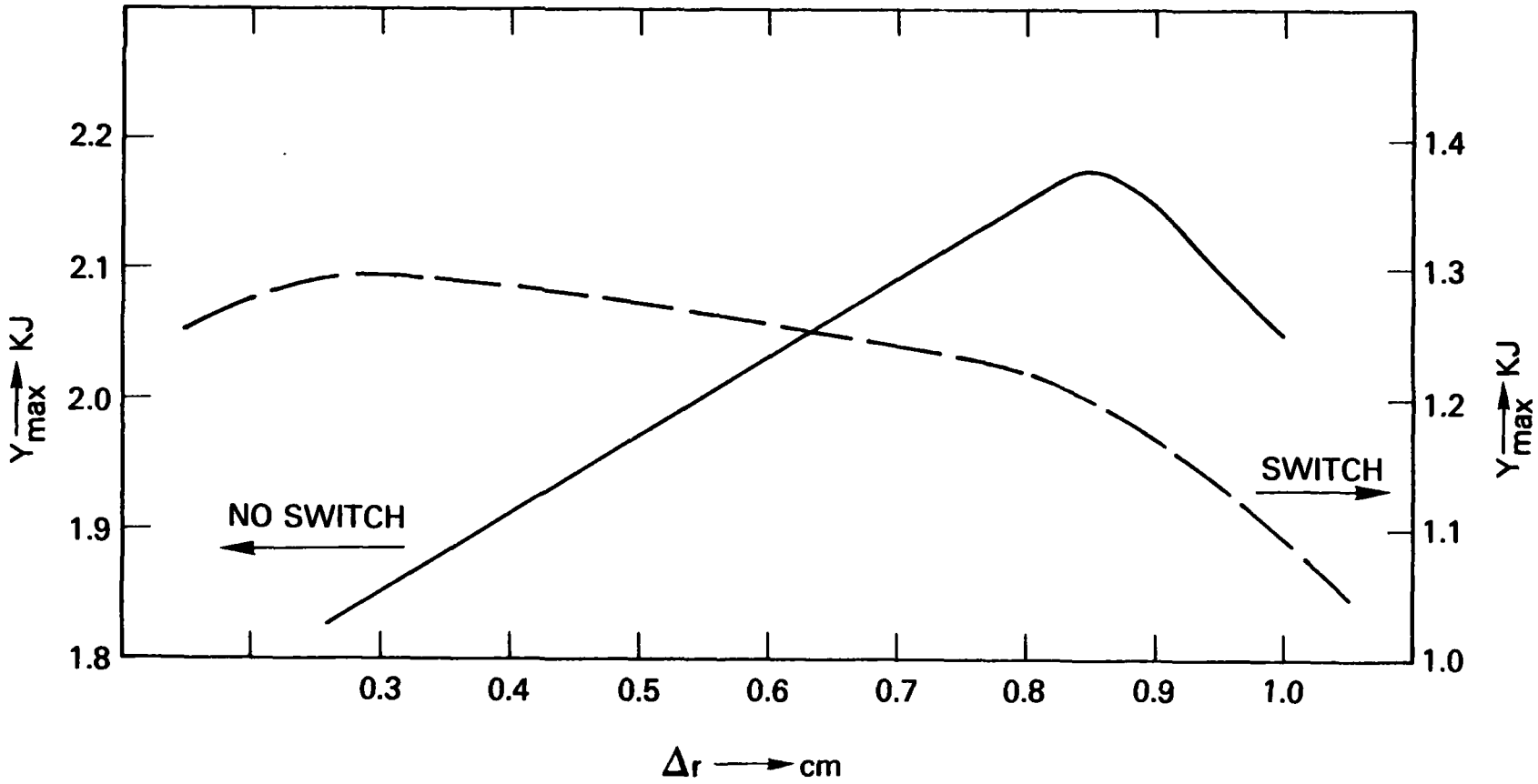

Fig. 24. Maximum Yield vs Shell Thickness for Fixed Mass.

REFERENCES

1. P. Burkhalter, J. Davis, J. Rauch, W. Clark, G. Dahlbacka, and R. Schneider, J.A.P. 50,705 (1979).

2. M. Gersten, J. E. Rauch, W. Clark, R. D. Richardson, and G. M. Wilkinson, Appl. Phys. Lett. 39,148 (1981).

3. D. Duston and J. Davis, J. Quant. Spec. Rad. Trans. 27, 267 (1982).

4. N. Krall and A. Trivelpiece, "Principles of Plasma Physics," McGraw Hill Book Co., N.Y. (1973).

5. J. Shearer, Phys. Fluids 19,1426 (1976).

6. S.J. Stepanakis, et. al., "Effects of Pulse Sharpening and Gas Puff Imploding Plasma," APS Plasma Physics Meeting, Boston, 1984.

DISTRIBUTION LIST

Assistant to the Secretary of Defense Atomic Energy Washington, D.C. 20301 ATTN: Executive Assistant	1 Copy
Defense Technical Information Center Cameron Station 5010 Duke Street Alexandria, Va 22314	2 copies
Director Defense Intelligence Agency Washington, D.C. 20301 ATTN: DT-1B R. Rubenstein	1 Copy
Director Defense Nuclear Agency Washington, D.C. 20305	
ATTN: DDST	1 copy
ATTN: TITL	4 copies
ATTN: RAEV	1 copy
ATTN: STVI	1 copy
Commander Field Command Defense Nuclear Agency Kirtland AFB, New Mexico 87115 ATTN: FCPR	1 Copy
Chief Field Command Livermore Division Department of Defense P.O. Box 808 Livermore, CA 94550 ATTN: FCPRL	1 Copy
Director Joint Strat TGT Planning Staff Offutt AFB Omaha, Nebraska 68113 ATTN: JSAS	1 Copy
Undersecretary of Defense for RSCH and ENGRG Department of Defense Washington, D.C. 20301 ATTN: Strategic and Space Systems (OS)	1 Copy

Deputy Chief of Staff for RSCH DEV and ACQ — 1 Copy
Department of the Army
Washington, D.C. 20301
ATTN: DAMA-CSS-N

Commander — 1 copy each
Harry Diamond Laboratories
Department of the Army
2800 Powder Mill Road
Adelphi, MD 20783
ATTN: DELHD-N-NP
ATTN: DELHD-R J. Rosado
ATTN: DELHD-TA-L (Tech. Lib.)

U.S. Army Missile Command
Redstone Scientific Information Center — 3 Copies
Attn: DRSMI-RPRD (Documents)
Redstone Arsenal, Alabama 35809

Commander — 1 copy
U.S. Army Missile Command
Redstone Arsenal, Alabama 35898
ATTN: DRCPM-PE-EA

Commander
U.S. Army Nuclear and Chemical Agency
7500 Backlick Road — 1 copy
Building 2073
Springfield, VA 22150
ATTN: Library

Commander — 1 Copy
Naval Intelligence Support Center
4301 Suitland Road, Bldg. 5
Washington, D.C. 20390
ATTN: NISC-45

Commander — 1 Copy
Naval Weapons Center
China Lake, California 93555
ATTN: Code 233 (Tech. Lib.)

Officer in Charge — 1 Copy each
White Oak Laboratory
Naval Surface Weapons Center
Silver Spring, Md. 20910
ATTN: Code R40
ATTN: Code F31

Air Force Weapons Laboratory — 1 Copy each
Kirtland AFB, New Mexico 87117
ATTN: SUL
ATTN: CA
ATTN: APL
ATTN: Lt. Col Generosa

Deputy Chief of Staff — 1 Copy
Research, Development and Accounting
Department of the Air Force
Washington, D. C. 20330
ATTN: AFRDQSM

Commander — 1 Copy
U.S. Army Test and Evaluation Command
Aberdeen Proving Ground, MD 21005
ATTN: DRSTE-EL

Space and Missile Systems Organization/SK — 1 Copy
Air Force Systems Command
Post Office Box 92960
Worldway Postal Center
Los Angeles, CA 90009
ATTN: SKF P. Stadler (Space Comm. Systems)

AVCO Research and Systems Group — 1 Copy
201 Lowell Street
Wilminton, MA 01887
ATTN: Library A830

BDM Corporation — 1 Copy
7915 Jones Branch Drive
McLean, Virginia 22101
ATTN: Corporate Library

Berkeley Research Associates — 1 Copy
P.O. Box 983
Berkeley, CA 94701
ATTN: Dr. Joseph Workman

Berkeley Research Associates — 1 Copy each
P.O. Box 852
5532 Hempstead Way
Springfield, VA 22151
ATTN: Dr. Joseph Orens
ATTN: Dr. Nino Pereira

Boeing Company — 1 Copy
P. O. Box 3707
Seattle, WA 98134
ATTN: Aerospace Library

The Dikewood Corporation — 1 Copy
1613 University Bldv., N.E.
Albuquerque, New Mexico 8710
ATTN: L. Wayne Davis

EG and G Washington Analytical Services Center, Inc. — 1 Copy
P. O. Box 10218
Albuquerque, New Mexico 87114
ATTN: Library

General Electric Company — 1 Copy
Space Division
Valley Forge Space Center
P. O. Box 8555
Philadelphia, PA 19101
ATTN: J. Peden

General Electric Company - Tempo — 1 Copy
Center for Advanced Studies
816 State Street
P.O. Drawer QQ
Santa Barbara, CA 93102
ATTN: DASIAC

Institute for Defense Analyses — 1 Copy
1801 N. Beauregard St.
Alexandria, VA 22311
ATTN: Classified Library

IRT Corporation — 1 Copy
P.O. Box 81087
San Diego, CA 92138
ATTN: R. Mertz

JAYCOR — 1 Copy
11011 Forreyane Rd.
P.O. Box 85154
San Diego, CA 92138
ATTN: E. Wenaas

JAYCOR — 1 Copy
205 S. Whiting Street, Suite 500
Alexandria, VA 22304
ATTN: R. Sullivan

KAMAN Sciences Corp. — 1 copy each
P. O. Box 7463
Colorado Springs, CO 80933
ATTN: J. Hoffman
ATTN: A. Bridges
ATTN: D. Bryce
ATTN: W. Ware

Lawrence Livermore National Laboratory — 1 copy each
University of California
P.O. Box 808
Livermore, California 94550
Attn: DOC CDN for L-153
Attn: DOC CDN for L-47 L. Wouters
Attn: DOC CDN for Tech. Infor. Dept. Lib.

Lockheed Missiles and Space Co., Inc. — 1 copy each
P. O. Box 504
Sunnyvale, CA 94086
Attn: S. Taimlty
Attn: J.D. Weisner

Lockheed Missiles and Space Co., Inc. — 1 Copy
3251 Hanover Street
Palo Alto, CA 94304
Attn: J. Perez

Maxwell Laboratory, Inc. — 1 Copy each
9244 Balboa Avenue
San Diego, CA 92123
ATTN: A. Kolb
ATTN: M. Montgomery
ATTN: J. Shannon

McDonnell Douglas Corp. — 1 Copy
5301 Bolsa Avenue
Huntington Beach, CA 92647
ATTN: S. Schneider

Mission Research Corp. — 1 Copy each
P. O. Drawer 719
Santa Barbara, CA 93102
ATTN: C. Longmire
ATTN: W. Hart

Mission Research Corp.-San Diego — 1 Copy
5434 Ruffin Rd.
San Diego, California 92123
ATTN: Victor J. Van Lint

Northrop Corporation — 1 Copy
Northrop Research and Technology Center
1 Research Park
Palos Verdes Peninsula, CA 90274
ATTN: Library

Northrop Corporation — 1 Copy
Electronic Division
2301 120th Street
Hawthorne, CA 90250
ATTN: V. Damarting

Physics International Company — 1 Copy each
2700 Merced Street
San Leandro, CA 94577
Attm: C. Stallings
Attn: C. Gilman

R and D Associates — 1 Copy each
P.O. Box 9695
Marina Del Rey, CA 90291
ATTN: W. Graham, Jr.
ATTN: P. Haas

Sandia National Laboratories — 1 copy each
P.O. Box 5800
Albuquerque, New Mexico 87115
ATTN: Doc Con For 3141
ATTN: D. McDaniel
ATTN: P. VanDevender
ATTN: K. Matzen, Code 4247

Science Applications, Inc. — 1 copy
P. O. Box 2351
La Jolla, CA 92038
ATTN: R. Beyster

Spire Corporation — 1 copy
P. O. Box D
Bedford, MA 01730
ATTN: R. Little

SRI International — 1 copy
333 Ravenswood Avenue
Menlo Park, CA 94025
ATTN: S. Dairiki

S-CUBED — 1 copy
P. O. Box 1620
La Jolla, CA 92038
ATTN: A. Wilson

Director
Strategic Defense Initiative Organization — 1 copy each
Pentagon 20301-7100
ATTN: Lt. Col Richard Gullickson/DEO
Dr. Dwight Duston

Texas Tech University — 1 copy
P.O. Box 5404
North College Station
Lubbock, TX 79417
ATTN: T. Simpson

TRW Defense and Space Systems Group — 1 Copy
One Space Park
Redondo Beach, CA 90278
ATTN: Technical Information Center

Vought Corporation — 1 Copy
Michigan Division
38111 Van Dyke Road
Sterling Heights, Maine 48077
ATTN: Technical Information Center
(Formerly LTV Aerospace Corp.)

Naval Research Laboratory
Plasma Radiation Branch
Washington, D.C. 20375

Code 4720 - 50 Copies
Code 4700 - 26 Copies
Code 2628 - 20 Copies

Director of Research
U.S. Naval Academy
Annapolis, MD 21402 — 2 Copies

DEPARTMENT OF THE NAVY

NAVAL RESEARCH LABORATORY
Washington, D.C. 20375-5000

OFFICIAL BUSINESS
PENALTY FOR PRIVATE USE, $300

POSTAGE AND FEES PAID
DEPARTMENT OF THE NAVY
DoD-316
THIRD CLASS MAIL

END

FILMED

9-85

DTIC